

96-81

Environment Canada

Water Science and
Technology Directorate

Direction générale des sciences
et de la technologie, eau

Environnement Canada

Farfield Mixing Characteristics of the Niagara River
Plume

By:

B.K. Pal, C.R. Murthy, and K. Miners

NWRI Contribution # 96-81

TD
226
N87
No. 96-
81

FARFIELD MIXING CHARACTERISTICS OF THE NIAGARA RIVER PLUME

B.K. Pal¹, C.R. Murthy² and K. Miners²

¹ Institute of Ocean Sciences
Sidney, British Columbia
Canada V8L 4B2

² Lakes Research Branch
National Water Research Institute
Burlington, Ontario
Canada L7R 4A6

MANAGEMENT PERSPECTIVE

The Niagara River is the major inflow into Lake Ontario, and delivers the bulk of suspended and dissolved material, including toxic substances, into the lake. Since the mixing of the Niagara River outflow within Lake Ontario has a critical impact on the water quality in the lake, there has been much concern about the transport, distribution, pathways and fate of toxic chemicals entering the lake via the Niagara River. The delineation of the physical mixing characteristics of the Niagara River Plume in Lake Ontario is essential to interpret the transport and distribution of the toxic contaminants within the lake.

The results presented in this report illustrate the farfield mixing of the Niagara River outflow by tracking river water masses using satellite-tracked Lagrangian drifters. The results document the remarkable variability of the Niagara River Plume in Lake Ontario, particularly the impact of the persistent south shore coastal current and the westward displacements of the plume. These observations correlate well with the distribution of sediment-borne toxic contaminants such as mercury and mirex attributed to the Niagara River outflow (Thomas 1983). The report provides a basis for the integration of the transport, distribution and pathways of toxic contaminants in the Niagara River-Lake Ontario-St. Lawrence River system.

Abstract

Historical data base of Lagrangian flow measurements from Lake Ontario, covering the period 1983-1990, is analysed with a view to understand turbulent exchange properties in the lake environment. The examination of individual drifter trajectories indicates that a diversity of flow fields ranging from jets to trapping regions (i.e., eddies) characterized by different length and time scales exist in the lake. Despite the nonuniform nature of the observations, we have assumed homogeneous and stationary fluctuations to calculate Lagrangian and Eulerian statistics. The computation of dispersion of single particles about the mean drift shows that the theory of diffusion by homogeneous random motion describes these dispersive motions quite well. Cluster analysis is also used to study diffusion produced by the eddies of the size of the drifter cluster. The Eulerian spatial and temporal correlations are calculated and compared with their Lagrangian counterpart.

1.0 Introduction

The Niagara River has been pinpointed as the major source of toxic contaminants in Lake Ontario (Thomas, 1983). Contamination enters the lake through the Niagara River discharge ($6500 \text{ m}^3 \text{ s}^{-1}$) that flows from Lake Erie to Lake Ontario, along the Canada-U.S. border. Highly toxic chemicals of industrial origin are found in the river as well as the lake through discharges from chemical plants and leaching from chemical dump sites. In recent years, there has been much concern in both United States and Canada about the fate of the toxic chemicals entering the lake.

During last one and a half decade, there have been a number of studies involving biological, chemical and physical properties of the Niagara River plume (e.g., Allan *et al.*, 1983). Most of the physical studies in Lake Ontario involve Eulerian measurements (Blanton, 1974a,b; Bull and Murthy, 1978; Boyce *et al.*, 1989; Masse and Murthy, 1990, 1992) and/or numerical modelling (Simons, 1974; Murthy *et al.*, 1986; Simons and Schertzer, 1989). From a theoretical stance, the Lagrangian measurements allow diffusion to be examined more realistically as it follows the water particles closely. However, very few studies exist on Lagrangian measurements in this lake. In fact, the first and only attempt to parameterize the mixing characteristics in Lake Ontario was by Murthy (1976), who investigated large scale horizontal diffusion characteristics by using fluorescent dye.

In the study of the dispersion of pollutants, plankton dynamics and numerical modelling a choice of proper value of horizontal eddy-diffusivity K_H is critical to the study. In most cases, researchers use the scale dependence relation suggested by Okubo (1971). However, the exact relationship between scale and rate of diffusion is not established. It is possible that there is no simple relationship between the eddy diffusivity and the scale of turbulence. In that sense it is important that as many observational estimates of K_H as possible be made in different environments.

In order to understand the transport, pathways and mixing of the toxic contaminants in Lake Ontario, the National Water Research Institute (NWRI) conducted a series of experiments during the period 1983-1985, June-October 1989 and May-November 1990. These experiments were part of an integrated project to map the near-field and far-field characteristics of the Niagara River plume in Lake Ontario. The near-field characteristics were studied by using conventional drifters and Electronic Bathymetry (EBT). Murthy *et al.* (1986) and Masse and Murthy (1990, 1992) studied the dynamics of the near-field characteristics of the Niagara River plume relating to the dispersion of river-borne contaminants in the lake. The mapping of the far-field characteristics of the Niagara River plume was done by tracking Lagrangian drifters by satellite over long periods of time. This report summarizes the far-field trajectory of the plume and its implications to transport and mixing of river borne toxic contaminants in Lake Ontario.

2.0 Experiments

Experiments consisted of daily thermal mapping surveys in which vertical profiles were taken at stations on a predefined grid, and daily drogue tracking surveys in which 10 drifters were released across the river mouth in the morning and tracked until evening by a small launch equipped with a Motorola Miniranger positioning system. When satellite-tracked drifters were released, each was launched at the recovery site of a conventional drifter which appeared to have stayed with the main part of the river plume. Thus, in the broadest sense, the satellite drifter tracks might be construed as a projected trajectory of Niagara River effluent.

The data base for this analysis originated from Argos satellite-tracked drifting buoys deployed at the Niagara River mouth in Lake Ontario. Drifting buoys deployed during 1983 and 1984 were provided by NOAA's Great Lakes Environmental Research Laboratory (GLERL) in Ann Arbor Michigan. NWRI acquired six Argos drifters in 1985, with further acquisitions in ensuing years, making it possible to conduct a number of drifter experiments at the Niagara River in Lake Ontario.

The design of NWRI drifters differed considerably from the GLERL ones (Fig. 1). The GLERL buoys, produced by Polar Research Laboratories (PRL), were of a spar-buoy type design about 1.5 m long, including the antenna housing. The upper portion of the main aluminum cylinder housed the Argos transmitter while the lower portion was occupied by batteries. A foam-filled floatation ring about 0.5 m in diameter attached to the upper main cylinder. A heavy lug provided attachment for a drogue at the bottom centre of the main cylinder. The NWRI buoys, manufactured by Hermes Electronics, consisted of upper and lower fiberglass shells about 0.6 m in diameter, bolted together to form an elliptical shaped buoy. The lower hull contained batteries and the transmitter fitted into hollows in foam filler. The upper shell was foam-filled except for a cavity at the centre to accommodate the short vertical antenna. A bridle slung from eye-bolts replacing four of the assembly bolts provided drogue attachment at its common point. A cylinder fitted with batteries and a flashing warning light was mounted on a special bracket fitted to one of the remaining assembly bolts. Its weight was offset by a length of chain slung from the eye-bolts on the opposite side of the buoy.

Roller-blind type drogues were used in all experiments. The early experiments employed the GLERL drogues which consisted of heavy rubberized canvas sails 1 m wide and 4 m high with metal spreaders top and bottom and supported by a chain bridle. Fitted to a PRL buoy, the drogue tracked at an effective depth of about 5 m. All later deployments used NWRI drogues which consisted of reinforced polyethylene tarpaulins 3 m wide and 2.4 m high, weighted at the bottom with 1.6 cm diameter reinforcing bar, and topped with 3 cm diameter aluminum pipe which provided attachment for a 4 mm wire rope bridle. The effective depth to the centre of these drogues was about 3.5 m on a PRL buoy. A depth adjustment link was added to Hermes drifters with this type of drogue to bring the effective depth to about 3.5 m.

The Argos satellite tracking system is a joint venture of space agencies of France and United States. NOAA TIROS satellites in near-polar orbits at about 850 km altitude carry the Argos instrumentation. Two such satellites in substantially different orbital planes operate simultaneously; each completing an orbital sweep of the earth in about 102 minutes. At any

given time, a satellite 'sees' a circular area of the earth's surface about 5000 km in diameter. In each revolution the earth's rotation results in a 25 degree apparent shift in the swath swept over by the satellite. This amounts to about 2800 km at the equator; hence, a considerable overlap in coverage. This geometry provides best coverage at the poles, with mean passes per day for two satellites varying from 7 at the equator to 28 at the poles. At our latitude ground stations 'see' the satellites about 10 to 11 times per day. Note that intervals between successive 'hits' can vary from a few minutes to several hours.

Users subscribe to use the Argos system for relaying data from and/or determining position of one or more platform transmitter terminals (PTT). Position, is determined from the Doppler shift in the stable 401.65 MHz frequency transmitted by the PTT- along with its ID code- at intervals of 100 seconds or less as assigned by Argos. The satellite must acquire several successive transmissions in a given pass to fix the PTT position. Each data message includes a location class which is derived from an assessment of the principal factors affecting position accuracy: number of messages received in the satellite pass; the time between the first and last message; PTT oscillator stability; and the PTT-satellite geometry at the time of the fix. The one standard deviation accuracies for location classes 1,2, and 3 are given as 1 km, 350 m, and 150 m respectively (Argos User's Manual). Information acquired for all legitimate PTT contacts is stored in the satellite memory until communication is established with one of several ground tracking stations, at which time data is downloaded to the tracking station and relayed to the redundant data processing centres in Toulouse, France, and Landover, U.S.A. Data is available from Argos in several forms (including directly monitoring the satellite if desired: not relevant to this work). On-line access to the data bank via modem and subscription to a data network, can retrieve the most recent message for a single PTT, or all of a user's data for today plus up to four previous days. Data is retained on the system for up to four months, during which time monthly tape, diskette, or printed copies may be acquired.

During experiments the current drifter positions for all active drifters were downloaded from the Argos computer at least once a day. These positions were plotted on lake charts, and an

assessment was made of the locations relative to shorelines, shoals, and the previous location for the same drifters. A drifter was usually left alone until it beached unless it had lost its drogue (detectable by a sudden increase in velocity), or its drogue was dragging bottom. Data for any such abnormal conditions was discarded.

3.0 Data

As described above, the raw Argos data consists of an irregular series of records, each consisting of PTT ID, time, position, and reference data. Data was received on standard 1200 ft (366 m) reels of 1/2 in (13 mm) magnetic tape with all data for a calendar month, arranged chronologically, for each buoy in succession according to increasing PTT ID number. The first phase of processing read the magnetic tape, and rewrote the data to a disk file in an abbreviated format which retained only ID, time, and position data. Redundant data were removed, and where fixes for the same buoy occurred closer together than 15 minutes, only the first one with the best position class was retained. The latter process was important because of the large errors possible later on when calculating velocities by dividing apparent change in position by the difference in time between fixes. Even for two consecutive high quality class 3 fixes taken 15 minutes apart, error velocities of the same order of magnitude as moderate lake currents would be quite possible without exceeding the predicted position errors. Since data tapes are monthly, and no attempt was made to delineate different missions for each drifter, the preliminary program also flagged time gaps larger than might ordinarily be expected between fixes. At the end of a year, a file of the whole year's data was created by first stacking all the edited monthly data files chronologically onto one file then using an editor to join all segments for each drifter. At this point the data was scanned again manually, removing any monthly delineation, and inserting markers delineating drifter missions. Finally, hourly data files for each drifter mission were generated by a program which inputs the irregular data to an interpolation routine devised by Akima (1972) of U.S. Department of Commerce. The output was an hourly time series, which when plotted would pass through all original data points. This

program also calculated, and output, hourly velocities. A further visual check of the velocity column of the output file revealed missed anomalies, such as a group of high velocities at the start or end of a mission where the drifter had been turned on before being transported to the release site, or had been left on for some time after recovery. One other program calculated displacements relative to the release site, and output hourly information in the format of standard NWRI current and meteorological files to enable the use of numerous programs for analysing data from those systems.

4.0 Theoretical Background

The basic drifter data available for our analysis consisted of positions of drifters at 60 minute intervals. The original sampling interval was nonuniform. The data was subsequently interpolated at 1 hour intervals by using the interpolation scheme of Akima (1972). Thus the position of the drifter is represented by

$$x_i = x_i(a_i, t) \quad i = 1, 2 \quad (1)$$

where a_i denotes i th component of the initial position of the drifter. The position time series was then converted to a velocity time series by using centre differencing technique. This resulted in two time series $u_i(t)$, ($i = 1, 2$), which were then used as basic data for further analysis.

The methods of computing Lagrangian statistics, Lagrangian scales of variability (e.g., Lagrangian Time and Length scales) and coefficients of eddy diffusivities have been put forward by a number of authors including Colin de Verdier (1983), Krauss and Bonning (1987), Poulain and Niiler (1989), Thomson *et al.* (1991) and Paduan and Niiler (1992). First, we investigate Lagrangian scales of variability from individual drifters. We then develop single-particle and cluster analyses.

Lagrangian Time and Length Scales

We follow Taylor's (1921) approach to examine the Lagrangian scale of variability and to describe diffusive transports by the eddy field. Taylor showed that, in stationary homogeneous turbulence field, the dispersion of tracers can be related to Lagrangian integral time scale through velocity autocorrelation. In spite of the nonstationary (nonstationarity is discussed later) and nonuniform nature of the observations, we begin the analysis with the assumption of stationary, homogeneous turbulence. The Lagrangian autocorrelation, R_{ii}^L , is generally defined as

$$R_{ii}^L(\tau) = \frac{1}{T} \frac{\int_0^{T-\tau} u_i'(t)u_i'(t + \tau)dt}{\langle u_i'^2 \rangle} \quad (2)$$

where u' is the residual velocity defined by $u' = u - \langle u \rangle$ and $\langle . \rangle$ denotes average over time. Division by the duration of the experiment T , rather than $T-\tau$ reduces the bias at large lags (Beauchamp and Yuen, 1979). The Lagrangian integral time scale (T_i^L) and length scale (L_i^L) are the time and the distance over which a drifter's motion remains correlated to itself. They are defined by

$$T_i^L = \int_0^T R_{ii}^L(\tau)d\tau, \quad (3)$$

$$L_i^L = \sqrt{\overline{u_i'^2}} \int_0^T R_{ii}^L(\tau)d\tau = \sqrt{\overline{u_i'^2}} T_i^L. \quad (4)$$

The components of the Lagrangian integral time and length scales are generally time dependent and do not approach a constant limit (see Pal and Sanderson (1992), Poulain and Niiler (1989)). There is a great deal of variability in the individual autocorrelation functions. Most of these

have significant negative lobes which under-estimate the integral time-scales as they are integrated over the entire duration of the experiment. To avoid this, we follow the usual practice of integrating from zero to the time of the first zero crossing (Thomson *et al.*, 1990; Poulain and Niiler, 1989). This can be viewed as the upper bounds to the true scales.

Single-Particle Dispersion

For homogeneous isotropic turbulence, the mean-squared dispersion of a single particle can be represented as (Taylor, 1921)

$$\langle x_i'^2(t) \rangle = 2 \langle u_i'^2 \rangle \int_0^t (t - \tau) R_{ii}^L(\tau) d\tau \quad (5)$$

where $\langle x_i'^2 \rangle$ is the mean-square dispersion in the i -direction due to u_i' and R_{ii}^L is the Lagrangian autocorrelation (3.2). The two important limiting cases for (3.5) are

$$\langle x_i'^2 \rangle = \langle u_i'^2 \rangle t^2, \text{ for } t \ll T_i^L \quad (6)$$

$$\langle x_i'^2 \rangle = 2 \langle u_i'^2 \rangle T_i^L t, \text{ for } t \gg T_i^L. \quad (7)$$

The results (3.6) and (3.7) state that the dispersion $\langle x_i'^2 \rangle^{1/2}$ is linear in time for t small compared to the integral time scale (initial dispersion regime). But for time t greater than the

integral time scale, $\langle x_i'^2 \rangle^{1/2}$ vary as $t^{1/2}$ (random-walk regime). In the random-walk regime, the eddy diffusivity is also given by

$$K_{ii} = \langle u_i'^2 \rangle T_i^L. \quad (8)$$

Cluster Analysis

Csanady (1973) noted that the theory of relative diffusion is the appropriate framework for the consideration of oceanic diffusion. In single-particle analysis, it is assumed that the motion of each particle in a group is independent of others. This is true if the initial separation of the diffusing particles is large compared with the integral scale of turbulence. For such case, there will be no correlation between the motions of the particles in the group and the particles move independently of each other. However, in most cases, drifters are deployed in a limited area with small separation between them. In that case, the motion of the particles in the cluster cannot be considered independent of the other particles. Besides, the absolute positions are not known with nearly the same precision as relative drifter positions and the position of the centre of gravity of the diffusing particles is not always well defined.

A method of practical importance is to consider relative diffusion where the increase in size of the group of particles is treated with respect to a frame of reference moving with the centre of gravity of the cluster. For small cluster size, only the eddies of the same size as the cluster participate in diffusing the cluster. Eddies of size larger than the cluster dimension transport the whole cluster and their motion is considered as mean field. The irregular displacement of the centre of gravity is described as meandering of the mean field. Thus the absolute diffusion includes both relative diffusion and meandering.

The Lagrangian autocorrelation function, R_H^r , for velocities relative to the centroid is given by

$$R_H^r(\tau) = \frac{1}{N} \frac{\sum_{n=1}^N \frac{1}{T} \int_0^{T-\tau} u_{in}^{/r}(t) u_{in}^{/r}(t + \tau) dt}{U_i^{/r} U_i^{/r}} \quad (9)$$

where $u_{in}^{/r}$ and $U_{in}^{/r}$ are the relative velocity and the root-mean-square velocity respectively. The integral time scale is calculated by integrating autocorrelation function from zero to the time of first zero-crossing as discussed before.

Eulerian Analysis

In previous sections, we considered Lagrangian statistics where drifter velocity was functions of Lagrangian coordinates $a = x(t = 0)$ and time t . Drifter velocity may also be specified as functions of fixed position x and time t i.e., Eulerian Coordinate system. (A current meter at position x and time t will measure the velocity identical to a drifter that passes through x at time t .) Thus it is the coordinate system in which we analyse drifter data that determines whether we obtain Lagrangian or Eulerian velocity statistics. In the following work, we discuss Eulerian statistics from spatio-temporal correlations. Again, the analysis is based on the assumption that velocity fluctuations are stationary and homogeneous. We follow Middleton and Garrett (1986) to develop the theory.

The joint space-time correlation of the x and y component of the residual velocities is given by

$$R_{ij}^J(r, \tau) = \overline{u_i'(x, t) u_j'(x + r, t + \tau)} V'^{-2} \quad (10)$$

where V'^2 denotes the component averaged velocity variance and the overbar represents averaging in both x and t . The x and t points may be either uniformly or randomly spaced. The Lagrangian equivalent of the Eulerian Cartesian correlation (3.10) is

$$\hat{R}_{ij}(r, \tau) = \langle u_i'(x(a, t), t) u_j'(y(b, t + \tau), t + \tau) \delta(x(b, t + \tau) - x(a, t) - r) \rangle V'^{-2} \quad (11)$$

where the averaging over the Lagrangian coordinates a and b do not include the same drifter (i.e., $a=b$). Assuming isotropy, the joint space-time correlation (3.10) may also be written as (Middleton and Garrett, 1986)

$$R_{ij}^J(r, \tau) = [f^*(r, \tau) - g^*(r, \tau)] r_i r_j / r^2 + \delta_{ij} g^* + \epsilon_{ij} h^*(r, \tau) \quad (12)$$

where $\epsilon_{11} = \epsilon_{22} = 0$, $\epsilon_{12} = -\epsilon_{21} = -1$, δ_{ij} is the Kronecker delta and f^* , g^* and h^* are the isotropic forms of the longitudinal, transverse and mixed correlations defined as

$$f^*(r, \tau) = \overline{u_L'(x, \tau) u_L'(x + r, t + \tau)} V'^{-2} \quad (13)$$

$$g^*(r, \tau) = \overline{u_N'(x, \tau) u_N'(x + r, t + \tau)} V'^{-2} \quad (14)$$

$$h^*(r, \tau) = \overline{\{u_L'(x, \tau)u_L'(x + r, t + \tau) - u_N'(x, \tau)u_N'(x + r, t + \tau)\}} (2V)^{-1} \quad (15)$$

u_L' and u_N' are the residual velocities that are longitudinal and transverse to the lag vector r respectively. The mixed correlation h^* is an Eulerian measure of the preferred sense of rotation.

Assuming that f^* and g^* are separable functions of r and τ , one can define spatial correlations

$$f(r) = \frac{\int_0^T N(r, \tau) f^*(r, \tau) d\tau}{f(0) \int_0^T N(r, \tau) d\tau} \quad (16)$$

$$g(r) = \frac{\int_0^T N(r, \tau) g^*(r, \tau) d\tau}{g(0) \int_0^T N(r, \tau) d\tau} \quad (17)$$

and time-lagged correlations

$$F(\tau) = \frac{\int_0^L N(r, \tau) f^*(r, \tau) dr}{F(0) \int_0^L N(r, \tau) dr} \quad (18)$$

where the correlations are normalized by the correlations at zero lag.

$$G(\tau) = \frac{\int_0^L N(r, \tau) g^*(r, \tau) dr}{G(0) \int_0^L N(r, \tau) dr} \quad (19)$$

5.0 Data Analysis

Two drifters were released on October 3, 1983 at a position slightly north-east of the Niagara River mouth and were tracked for 14 days. They were then recovered, checked and redeployed on October 20, slightly west of the previous position and were tracked for another 10 days. Figures 3.1a and 3.1b show their trajectories. The trajectories reveal a complex flow pattern. In Figure 3.1a, although the two drifters were released at the same point and at the same time, their tracks are totally different showing the dominance of the small scale turbulent motion in the lake. In the second deployment (Figure 4.1b), the two drifters followed a counter clockwise complex circulation before they were caught in the eastward flowing coastal jet.

Table 2 shows the mean and rms velocities, integral time-scale and eddy-diffusivities from the individual drifter tracks. The mean current along x(east) and y(north)-directions were (7.47 ± 5.22) and (1.21 ± 0.67) cm s⁻¹ respectively. These indicate that the flow is strongly anisotropic. The residual velocities were obtained by removing the mean velocity for each drifter. A representative plot of the components of the Lagrangian autocorrelation from the individual drifters are shown in Figure 4. There is a great deal of variability in the individual autocorrelation functions. Most of these have significant negative lobes and high frequency oscillations. The integral time scale is calculated using (3), the upper limit of integration is being taken as the first zero crossing as discussed earlier.

Two drifters were deployed on October 16, 1984, this time, at the mouth of the Niagara River and were tracked for 16 to 35 days. Figure 5 shows the two drifter trajectories. The trajectories show paths different from the previous trajectories (Fig. 3). The two drifters moved

offshore and swept across the western part of the basin in a semi-circular path. Then they turned right and followed the coastline. One drifter went ashore two weeks after deployment while the other, having moved slightly offshore, continued its journey eastward. Table 3 summarizes the mean and rms velocities, integral time scale and eddy diffusivities from the individual drifters. In the 1983 experiment, the Lagrangian integral time scales are 22.4 ± 10.2 and 7.4 ± 2.6 hours respectively in the x and y directions. In 1984, the x, y components of residual motion have integral time scales 30.0 ± 3.0 and 11.3 ± 6.5 hours respectively. The kinetic energies of the residual velocities were $259.5 \text{ cm}^2 \text{ s}^{-2}$ in 1983 and $140.9 \text{ cm}^2 \text{ s}^{-2}$ in 1984. Thus higher kinetic energies are associated with shorter integral time-scales. This is also observed by Krauss and Bonning (1987), Sanderson and Pal (1990) and Pal and Sanderson (1992). Sanderson and Pal (1990) provide a dimensional explanation for this result.

Two experiments were conducted in 1985 - one in June and the other in September close to the Niagara River mouth. Four drifters were used in the June experiment and five in the September experiment. The duration of the drifter trajectories range from 10 to 63 days. Figures 6a and 6b show the drifter trajectories of the two deployments. In the September experiment (Fig. 6b), although the drifters were deployed close together and at approximately the same time, the individual drifter trajectories vary widely. This suggests the dominance of the small scale turbulence and their complex interaction with the larger scale circulation. Only one drifter followed the southern coastline, whereas the other four drifters followed a very complex path and moved offshore and spread over the western part of the lake. These contrast with the June Experiment where all four drifters followed the coastal boundary current (Fig. 6a). This is a classic example of the extent of variability of turbulence in the lake current. The September 1985 Experiment will be further analysed to include cluster and Eulerian analysis.

Mean and rms velocities, integral time scales and eddy diffusivities from individual trajectories of the two experiments are summarized in Tables 4 and 4b.

Single-Particle Analysis

As mentioned earlier, the September 1985 experiment provides an example showing the dominance of the small scale turbulence and their complex interaction with the large scale circulation. We apply the single particle analysis on this data and examine the validity of the Taylor's hypothesis.

The determination of meaningful result requires averaging over a large number of independent drifter tracks in order to obtain reliable statistics from the drifter data. The number of drifters available for single-particle analysis is small and does not approach the large number of realizations required to determine meaningful single-particle statistics. The data base however may be increased by using the method first described by Colin de' Verdiere (1983) and later used by many others (e.g., Krauss and Boning, 1987; Poulain and Niiler, 1989; Thomson *et al.*, 1991). The upper limit of the integral time scale obtained from the individual trajectories was about 20 hours (see Table 4b). The velocities of the same drifter separated by more than 20 hours may be considered as independent and the position can be treated as the origin of a new track. The data base may therefore, be increased substantially by restarting the drifters every 20 hours.

Colin de Verdiere (1983) noted that, splitting the drifter trajectories in this way, the expected increase in the number of degrees freedom is less than the theory predicts. In order to avoid spurious statistics from the unwanted correlation between the drifter segments, we take decorrelation time scale $T=100$ hours which is roughly 5 times the mean integral time-scale. Thus the time series of hourly positions of the individual drifters were split up into a number of time series of 100 hours long without overlapping. End segments shorter than 100 hours are not incorporated in the analysis.

To derive single-particle statistics it is essential to remove the background circulation (i.e., centroid motion) from the drifter trajectories. The dispersion is thus estimated from the

cumulative effect of the motion due to turbulence. This yields a total of 32 pseudo drifter trajectories of 100 hours long all emanating from the same location (Figure 7). The mean and standard deviations of pseudo tracks are also shown as a function of time. The standard deviation of the positional fluctuations about the mean are observed to grow slowly with time. Figure 8 shows the plot of the mean square dispersion versus time and theoretical slopes of the random walk regime. The rms dispersion for the first 25 hours and slopes of initial dispersion is plotted in Figure 9. Although the general agreement between theoretical and observed curves in the random walk regime is good (Figure 8), it is not very encouraging in the initial dispersion regime (Figure 9).

Table 4b shows the single-particle statistics of the combined data set. The mean motion and eddy diffusivities appear smaller than those calculated from individual drifters whereas integral time scale and rms velocity vary by a small amount. The different means taken out (in the case of individual drifter analyses) and use of segmented tracks with discarded end segments are the cause of this discrepancy.

The autocorrelation function and coefficients of eddy diffusivities for single-particle analysis are shown in Figure 10. Eddy diffusivities show a tendency to saturate after 40 - 50 hrs reaching maximum values in the random walk regime of $K_{11} = 9.9 \times 10^6$, $K_{22} = 1.7 \times 10^6 \text{ cm}^2 \text{ s}^{-1}$. The corresponding length scales are 10.0 km and 21.0 km.

Cluster Analysis

Cluster analysis is performed on the September 1985 Experiment. Unlike the other experiments, the drifters followed a complex path and scattered over the entire lake. This gives us an opportunity to study the cluster scale turbulence by examining the relative motion with respect to the centre of gravity of the cluster.

The five drifters have slightly different starting times and ending times. Data is edited so that all five drifters start at the same time (i.e., on September 18 at 1000 GMT) and also end at the same time (i.e., on October 14 at 1900 GMT). By doing so we lose some data but it is very insignificant (less than 1%).

Figure 11 plots the drifter trajectories with respect to the cluster centroid and Figure 12 plots the centroid velocity versus time. Centroid velocity is large along x-direction with maximum and minimum of 55.0 cm s^{-1} to -25 cm s^{-1} compared to y-direction which varies from $28 \text{ cm}^2 \text{ s}^{-1}$ to $-23.0 \text{ cm}^2 \text{ s}^{-1}$. These are much larger than the average velocities obtained from single-particle motion (see Table 4b). Centroid velocities are superpositions of time-averaged mean current and any other high frequency motions that have space scales larger than the cluster dimensions.

Table 4b summarizes the statistics of the cluster analysis. The relative velocity field is anisotropic, the rms $u_i r^i$ ($i = 1, 2$) = (12.3, 8.2) cm s^{-1} , being mostly along x-direction. The ratio of the kinetic energy relative to the centroid to the kinetic energy for single-particle motion is 0.58. Clearly much of the single-particle motion analysed in previous section has length scales much greater than the cluster dimension and therefore contribute more to the centroid motion than to the relative motion. The Lagrangian autocorrelation function for velocities relative to the centroid is calculated using equation 9. Figure 13 shows the autocorrelation function and the eddy diffusivities as a function of time lag. The x- and y- component of the autocorrelations show oscillations. Therefore, integral time scale is calculated by integrating the autocorrelation function up to the first zero crossing. The integral time scale and eddy diffusivities are smaller than the single-particle estimates. These are consistent with the findings of Middleton and Garrett (1986) and others.

Eulerian Analysis

The September 1985 experiment is also examined from the Eulerian point of view. We will consider relative coordinate system where the origin is attached to the centre of mass of the patch. Assuming stationarity and homogeneity, the Eulerian ensemble average of the relative velocity $\overline{V_i^2}$ is replaced by the simple average over all drifter data (Middleton and Garrett, 1986). To calculate f^* , g^* , h^* , relative velocity pairs of distinct drifters were binned for space and time lags centred on $[r_1, r_2, r_3, \dots] = [0, 5, 10, \dots]$ km and $[\tau_1, \tau_2, \tau_3, \dots] = [1, 2, 3, \dots]$ h. The mixed correlation h^* fluctuated about zero and were close to zero indicating no dominant sense of eddy rotation. Figure 14 shows the plots of f^* and g^* . The patterns of relative correlations are complicated, however, they reveal some clear structures. Figure 14 shows that there is a tendency for negative correlations when space lags are large and time lags are relatively small and positive correlations at small space lags. This type of feature is also observed by Sanderson and Pal (1990) in the Atlantic Equatorial Undercurrent. They associated these with the eddy features that have space scales similar to the cluster dimension. The alternating signs of correlations on the τ -axis represent wave activities.

Assuming that f^* and g^* are separable functions of r and t , we can use equations 16 - 19 to calculate $f(r)$, $g(r)$ and $F(\tau)$, $G(\tau)$. Figures 15 and 16 show the plots of $f(r)$, $g(r)$ and $F(\tau)$, $G(\tau)$ respectively. The plot of $f(r)$ and $g(r)$ (Figure 4.13) shows positive correlation at smaller space lags and negative correlation at larger space lags. The resolution of space correlations is poor, as there are small number of drifters in the patch. Hence the zero crossings for f and g are not well determined. The plots of $F(\tau)$ and $G(\tau)$ (Fig. 16) demonstrate wave activities. The Eulerian integral time and space scales of the longitudinal and transverse velocities are calculated by integrating $f(r)$, $g(r)$ and $F(\tau)$, $G(\tau)$ up to the first zero crossing. The Eulerian integral time and space scales of the longitudinal and transverse velocities are:

$T_L^E = 18.8$ hr, $T_T^E = 18.1$ hr, $L_L^E = 4.0$ km, and $L_T^E = 15.2$ km. These are slightly larger in magnitude than those of cluster analysis estimates. This may be due to longitudinal and transverse velocities being more 'lined up' with the eddy causing the relative motion than the x - y coordinates as pointed out by Sanderson and Pal (1990).

6.0 Summary

Trajectories of satellite-tracked drifters with drogues set at 3.5 m depth were used to describe the pathways and farfield mixing properties of the Niagara River discharge in Lake Ontario. The dominating effect of large scale circulation features, such as the year-round belt of strong south-shore boundary current is clearly evident in the data; however, as Fig. 3, 5, and 6 illustrate, the farfield mixing shows remarkable variability. The correlation between the observed farfield mixing characteristics traced by the drifters, and the distribution of Mirex and mercury in bottom sediments of Lake Ontario (Thomas 1983) is striking. The mercury distribution in Fig. 17 shows higher concentrations corresponding to the persistent south-shore current, and to the periodic westward sweep of the Niagara River plume.

Despite the nonuniform nature of the drifter observations, we have assumed homogeneous and stationary fluctuations to calculate Lagrangian and Eulerian statistics. The drifter trajectories did not completely resemble random walk, but the cumulative effect of all the processes was dispersive. In that sense the estimates were reasonable and representative.

The drifter trajectories reveal that a diversity of flow fields, ranging from jets to eddies, comprise the lake circulation. The Lagrangian analysis of individual trajectories show that the fluctuations in the mean flow have an rms velocity of $u = (17.0, 10.0)$ cm s⁻¹ and integral time scales of 25.6 and 8.8 hr along zonal and meridional directions.

Single-particle and cluster analyses were carried out on September 1985 data. In the random walk regime, the agreement between Taylor's theorem and observations is reasonably good. However, in the initial regime, the mean dispersion is less than predicted; presumably due to proximity of the coastline (Poulain and Niiler, 1989). The rms velocity of the single-particle motion is u_i ($i = 1, 2$) = (16.3, 10.6) cm s⁻¹ which is close to the estimates from the individual trajectory analysis. The integral time scale ($x = 17.2$, $y = 5.5$) hr and eddy diffusivity K_{11}

$= 164.5$, $K_{22} = 22.0$) $\text{cm}^2 \text{ s}^{-1}$ are significantly smaller than those of the individual trajectory analysis.

Cluster analysis shows that the energy of turbulent motion is smaller (by a factor of 0.58) than that of the single-particle case indicating that a significant amount of the energy of single particle motion comes from the eddies that have space scales larger than the scale of the cluster. The integral time scale and eddy diffusivities from the cluster analysis are: $x = 16.1 \text{ hr}$, $y = 3.2 \text{ hr}$, $K_{11} = 99.1 \times 10^7 \text{ cm}^2 \text{ s}^{-1}$, $K_{22} = 16.8 \times 10^7 \text{ cm}^2 \text{ s}^{-1}$.

The estimates of Eulerian time scales are larger than those of single-particle analysis and cluster analysis. This is consistent with the findings of Middleton and Garrett (1986) and many others.

The types of analysis described here, and their results, are essential to the development of reliable models capable of predicting the mixing characteristics of substances released into natural waters.

REFERENCES

- Akima, H., Interpolation and smooth curve fitting based on local procedures, Communication of the ACM, 15(10), 914-918, 1972.
- Allan, R.J., A. Murdoch, and A. Sudar, An introduction to the Niagara River/Lake Ontario pollution problem, J. Great Lakes Res., 9, 111-117, 1983.
- Beauchamp, K., and C. Yuen, Digital Method for Signal Analysis, George Allen and Unwin, London, 316 pp, 1979.

- Blanton, J.O., Some characteristics of nearshore currents along the north shore of Lake Ontario, J. Phys. Oceanogr., 4, 415-424, 1974a.
- Blanton, J.O. and C.R. Murthy, Observations of lateral shear in the nearshore zone of a Great Lake, J. Phys. Oceanogr., 4, 660-663, 1974b.
- Boyce, F.M., M.A. Donelan, P.F. Hamblin, C.R. Murthy and T.J. Simons, Thermal structure and circulation in the Great Lakes, Atmosphere-Ocean, 27(4), 607-642, 1989.
- Bull, J.A. and C.R. Murthy, Climatology and structure of coastal currents in Lake Ontario during winter, report, 72 pp., Environ. Can., Natl. Water Res. Inst., Burlington, Ont., 1980.
- Colin De Verdiere, A., Lagrangian eddy statistics from surface drifters in the eastern North Atlantic, J. Mar. Sc., 41, 375-398, 1983.
- Csanady, G.T., Circulation in the coastal ocean, D. Reidel Publ. Co., Dordrecht, Holland, pp. 277, 1982.
- Csanady, G.T., Turbulent diffusion in the environment, D. Reidel Publishing Comp., pp. 248, 1973.
- Frank, R., R.L. Thomas, M. Holdrinet, A.L.W. Kemp and M E. Braun, Organochlorine insecticides and PCBs in surficial sediments (1968) and sediment cores (1976) from Lake Ontario, J. Great Lakes Res., 5, 18-27, 1979.
- Garrett, C., J.F. Middleton, F. Majaess, and M. Hazen, Analysis and prediction of iceberg trajectories. Department of Oceanography, Dalhousie University, Nova Scotia, 86 pp, 1985.

- Kanasewich, E.R., Time sequence analysis in Geophysics. The university of Alberta press, pp. 364, 1980.
- Krauss W. and C.W. Boning, Lagrangian properties of eddy fields in the northern north Atlantic as deduced from satellite-tracked buoys. J. Mar. Res., 45, 259-291, 1987.
- Masse, A.K. and C.R. Murthy, Observations of the Niagara River plume, J. Geophys. Res., 95(C9), 16097-16109, 1990.
- Masse, A.K. and C.R. Murthy, Analysis of the Niagara River plume dynamics, J. Geophys. Res., 97(C2), 2403-2420, 1992.
- Middleton, J.F. and C. Garrett, A kinematic analysis of polarized eddy fields using drifter data, J. Geophys. Res., 91, 5094-5102, 1986.
- Murthy, C.R., Horizontal diffusion characteristics in Lake Ontario, J. Phys. Oceanogr., 6, 76-84, 1976.
- Murthy, C.R. and Dunbar, Structure of the flow within the coastal boundary layer of the Great Lakes, J. Phys. Oceanogr., 11, 1567-1577, 1981.
- Murthy, C.R., T.J. Simons and D.C L. Lam, Dynamic and transport modelling of the Niagara River plume in Lake Ontario, Rapp. P.V. Reun, Cons. Int. Explor. Mer, 186 pp. 150-164, 1986.
- Murthy, C.R. and K. Miners, Mixing characteristics of the Niagara River plume in Lake Ontario, Water Pollution Res. J. Canada, 24, 143-162, 1989.
- Mysak, L.A., Topographically trapped waves, Ann. Rev. Fluid Mech., 12, 45-76, 1980.

- Okubo, A., Ocean diffusion diagrams, *Deep-Sea Research*, 18, 789-802, 1971.
- Paduan, J.D. and P P. Niiler, Structure of velocity and temperature in the northeast Pacific as measured with Lagrangian drifters in Fall 1987, *J. Phys. Oceanogr.*, 23, 585-600, 1993.
- Pal, B.K. and B.G. Sanderson, Measurements of drifter cluster dispersion, *Atmosphere-Ocean*, 30, 621-651, 1991.
- Poulain, P.M. and P.P. Niiler, Statistical analysis of the surface circulation of the California Current System using satellite-tracked drifters, *J. Phys. Oceanogr.*, 19, 1588-1603, 1989.
- Sanderson, B.G. and B.K. Pal, Patch diffusion computed from Lagrangian data, with application to the Atlantic Equatorial Undercurrent. *Atmosphere-Ocean.*, 28, 444-465, 1990.
- Simons, T.J., Verifications of Numerical models of Lake Ontario: I, Circulation in spring and early summer, *J. Phys. Oceanogr.*, 4, 507-523, 1974.
- Simons, T.J., Verifications of Numerical models of Lake Ontario: II, Stratified circulations and temperature changes, *J. Phys. Oceanogr.*, 5, 98-110, 1975.
- Simons, T.J. and W.M. Schertzer, The circulation of Lake Ontario during the summer of 1982 and the winter of 1982/83, *Natl. Water Res. Inst. Sc. Sr. No. 171*, 191 pp., Burlington, Ont., 1989.
- Taylor, G.I., Diffusion by continuous movements, *Proc. London Math. Soc.* A20, 196-211, 1921.

Thomas, R. L., Lake Ontario Sediments as indicators of the Niagara River as a primary source of contaminants, J. Great Lakes Res., 9, 118-124, 1983.

Thomson, R.E., P.H. LeBlond, and W.J. Emery, Analysis of deep-drogued satellite-tracked drifter measurements in the northeast Pacific, Atmosphere-Ocean, 28, 409-443, 1990.

Winant, C.D., and R.C. Beardsley, A comparison of some shallow wind-driven currents, J. Phys. Oceanogr., 9, 218-220, 1979.

FIGURE CAPTIONS

- Fig. 1: Schematic diagram of satellite-tracked drifting buoys.
- Fig. 2: Map of Lake Ontario showing location of the experiment sites.
- Fig. 3: Trajectories of surface drifters deployed on (a) October 3, 1983 and (b) October 20, 1983. The launch position is indicated by '+' and end position by '*'.
- Fig. 4: Zonal (solid) and meridional (dashed) Lagrangian autocorrelation versus time lag for drifter No. 3389.
- Fig. 5: Trajectories of surface drifters deployed on October 16, 1984. The launch position is indicated by '+' and end position by '*'.
- Fig. 6: Trajectories of surface drifters deployed on (a) June 5, 1985 and (b) Sept 18, 1985. The launch position is indicated by '+' and end position by '*'.
- Fig. 7: (a) Zonal and meridional displacements versus time after deployment of 32 segmented drifter tracks from September 1985, experiment. (b) The mean displacements (solid line) and associated rms intervals (dotted envelopes) are also shown.
- Fig. 8: Plot of mean-square dispersion versus time for the random walk regime. Symbols (triangle = zonal, cross = meridional) represent the observations. Taylor's theorem (eqn. 3.7) predicts the dispersion depicted by the solid line.

- Fig. 9: Plot of root-mean-square dispersion versus time for the initial dispersion regime. Symbols (triangle = zonal, cross = meridional) represent the observations. Taylor's theorem (eqn. 6) predicts the dispersion depicted by the solid line.
- Fig. 10: Lagrangian autocorrelation functions and diffusivities as a function of time lag for the (a) zonal and (b) meridional directions. (Single-particle analysis.)
- Fig. 11: Positions of drifters relative to the cluster centroid for September 1985 experiment.
- Fig. 12: Plot of velocity time series of the cluster centroid.
- Fig. 13: Lagrangian autocorrelation functions and eddy diffusivities as a function of time lag for the (a) zonal and (b) meridional directions. (Cluster analysis.)
- Fig. 14: Contour plots of Eulerian correlations f^* and g^* as functions of time and space lags, for September 1985 experiment. Areas of positive and negative correlations are designated by solid and dashed lines.
- Fig. 15: Plots of Eulerian spatial correlations f and g as functions of space lag. Error bars represent $\pm\sigma$ about the mean value.
- Fig. 16: Plots of Eulerian temporal correlations F and G as functions of time lag. Error bars represent $\pm\sigma$ about the mean value.
- Fig. 17: Distributions of Mirex and mercury in Lake Ontario sediments (from Thomas (1983)).

Table 1: Details of Buoy Deployment

Buoy ID	Launch			Recovery		
	Date/ time*	Latitude (north)	Longitude (west)	Date/ time*	Latitude (north)	Longitude (west)
3387	83/10/03/22	43.354	78.928	83/10/18/21	43.491	78.834
3389	83/10/03/22	43.353	78.927	83/10/18/18	43.599	77.900
3387	83/10/20/09	43.328	79.116	83/10/29/23	43.389	78.087
3389	83/10/20/09	43.330	79.112	83/10/29/18	43.372	77.840
3386	84/10/16/00	43.344	79.089	84/11/01/00	43.360	77.904
3388	84/10/16/00	43.344	79.098	84/11/20/00	43.392	77.282
2493	85/06/04/22	43.338	79.119	85/06/15/10	43.353	76.961
2498	85/06/05/00	43.347	79.124	85/07/08/20	43.704	76.234
3386	85/06/05/19	43.419	79.133	85/08/08/11	43.970	77.947
3388	85/06/05/00	43.369	79.131	85/06/14/18	43.290	77.229
2493	85/09/17/20	43.293	79.113	85/10/14/19	44.088	76.730
3386	85/09/18/07	43.316	79.158	85/10/18/07	43.984	77.920
3388	85/09/18/07	43.349	79.096	85/10/18/20	43.959	77.604
5380	85/09/18/10	43.319	79.167	85/10/14/19	43.799	78.951
5381	85/09/18/10	43.355	79.111	85/10/15/21	43.767	78.814

* year/month/day/hour GMT

Table 2: Mean and rms velocities, integral time and length scales, and eddy diffusivities from individual drifters for 1983 experiment.

Buoy ID	Mean U (cm/s)	Mean V (cm/s)	rms u (cm/s)	rms v (cm/s)	Tx (Hr)	Ty (Hr)	Lx (km)	Ly (km)	Kx $\times 10^5$ cm ² /s	Ky $\times 10^5$ cm ² /s
3387	0.6	1.2	15.8	11.2	9.4	3.6	5.3	1.4	83.9	16.1
3389	6.5	2.2	22.3	12.6	19.3	8.4	15.5	3.8	380.0	48.2
3387	10.0	0.9	20.4	8.2	30.5	8.8	22.4	2.6	456.4	21.3
3389	12.7	0.6	23.3	8.2	30.5	9.0	25.6	2.4	596.1	21.4
Mean	7.5 ± 5.2	1.2 ± 0.7	20.5 ± 3.3	10.0 ± 2.2	22.4 ± 10.2	7.4 ± 2.6	16.5 ± 1.2	2.7 ± 0.2	379.1 ± 216.2	26.8 ± 14.5

Table 3: Mean and rms velocities, integral time and length scales, and eddy diffusivities from individual drifters for 1984 experiment.

Buoy ID	Mean U (cm/s)	Mean V (cm/s)	rms u (cm/s)	rms v (cm/s)	Tx (Hr)	Ty (Hr)	Lx (km)	Ly (km)	Kx $\times 10^5$ cm ² /s	Ky $\times 10^5$ cm ² /s
3386	6.9	0.2	15.1	9.9	37.3	15.9	20.2	5.7	304.3	56.0
3388	4.9	0.2	10.8	11.6	22.7	6.6	8.8	2.8	115.4	27.9
Mean	5.9 ± 1.5	0.2 ± 0.0	12.9 ± 3.0	10.7 ± 1.2	30.0 ± 10.3	11.3 ± 6.5	14.0 ± 1.1	4.4 ± 0.3	209.9 ± 133.6	42.0 ± 19.9

Table 4a: Mean and rms velocities, integral time and space scales, and eddy diffusivities from individual drifters for June 1985 experiment.

Buoy ID	Mean U(cm/s)	Mean V(cm/s)	rms u(cm/s)	rms v(cm/s)	Tx (Hr)	Ty (Hr)	Lx (km)	Ly (km)	Kx $\times 10^5$ cm ² /s	Ky $\times 10^5$ cm ² /s
2493	19.3	0.5	17.3	7.7	20.4	4.0	12.7	1.1	219.6	8.5
2498	8.0	1.5	23.7	12.7	24.8	6.5	21.2	3.0	501.7	37.3
3386	1.7	1.1	16.1	9.4	49.8	13.5	28.4	4.5	463.0	42.5
3388	18.4	-0.8	18.4	8.6	15.1	3.9	10.0	1.2	183.6	10.4
Mean	11.8 ± 7.3	0.6 ± 0.9	18.9 ± 2.9	9.6 ± 1.9	27.5 ± 13.3	7.0 ± 3.9	18.7 ± 1.4	2.4 ± 0.3	342.0 ± 141.6	24.7 ± 15.3

Table 4b: Mean and rms velocities, integral time and space scales, and eddy diffusivities from individual drifters, single-particle and cluster analyses for September 1985 experiment.

Buoy ID	Mean U (cm/s)	Mean V (cm/s)	rms u (cm/s)	rms v (cm/s)	Tx (Hr)	Ty (Hr)	Kx $\times 10^5$ cm ² /s	Ky $\times 10^5$ cm ² /s
2493	8.2	3.9	16.4	7.6	18.5	26.4	178.6	55.4
3386	3.8	2.9	14.9	9.4	33.0	7.4	261.5	23.5
3388	4.5	2.6	14.3	12.0	11.5	3.7	85.1	19.0
5380	0.8	2.3	19.8	11.5	27.7	3.7	391.4	17.6
5381	1.0	1.9	17.4	11.2	21.3	7.1	231.1	31.6
Mean	3.7 ± 2.7	2.7 ± 0.7	16.6 ± 2.0	10.3 ± 1.6	22.4 ± 7.4	9.7 ± 8.5	229.5 $\pm 101.$	29.4 ± 13.9
Comb.*	4.6	2.7	16.3	10.6	17.2	5.5	164.5	22.0
Cluster			12.3	8.2	16.1	3.2	99.1	16.8

*combined 32 100 hour segments

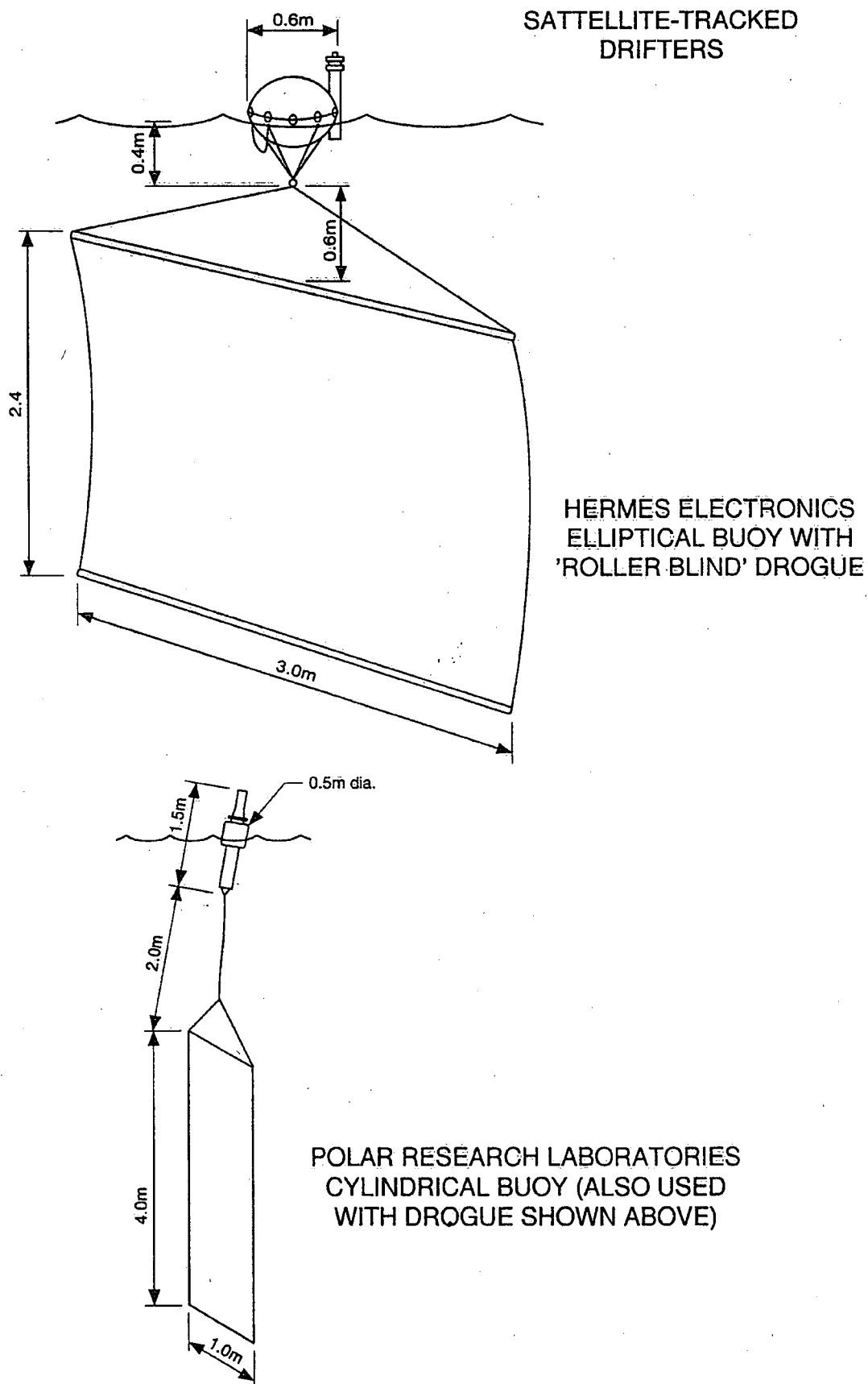


Fig. 1: Schematic diagram of satellite-tracked drifting buoys.

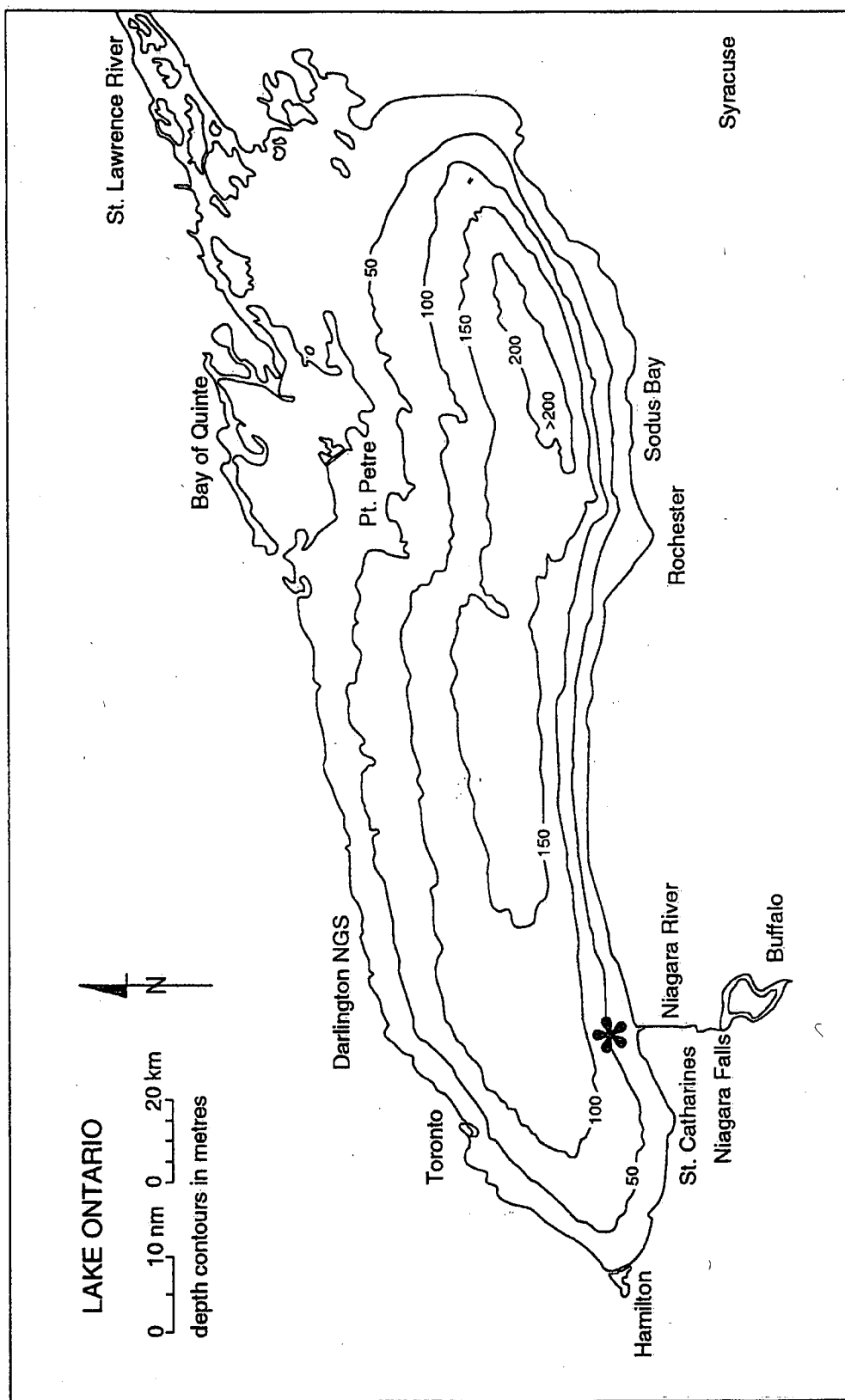


Fig. 2: Map of Lake Ontario showing location of the experiment sites.

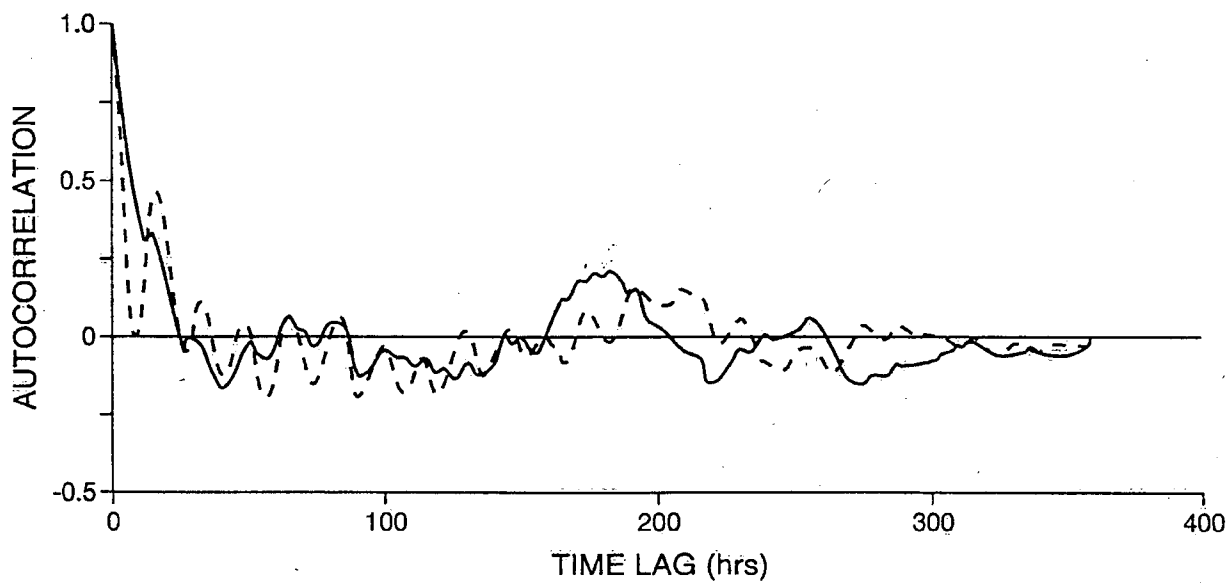


Fig. 4: Zonal (solid) and meridional (dashed) Lagrangian autocorrelation versus time lag for drifter No. 3389.

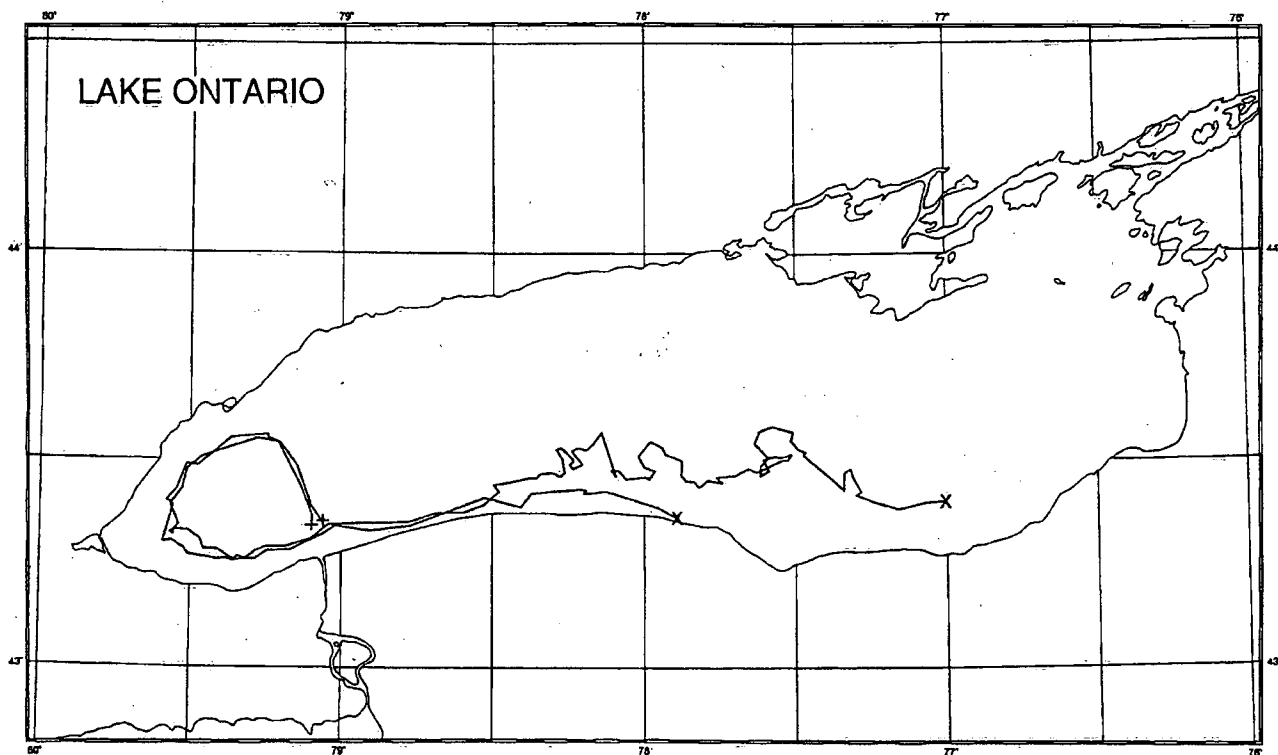


Fig. 5: Trajectories of surface drifters deployed on October 16, 1984. The launch position is indicated by '+' and end position by 'x'.

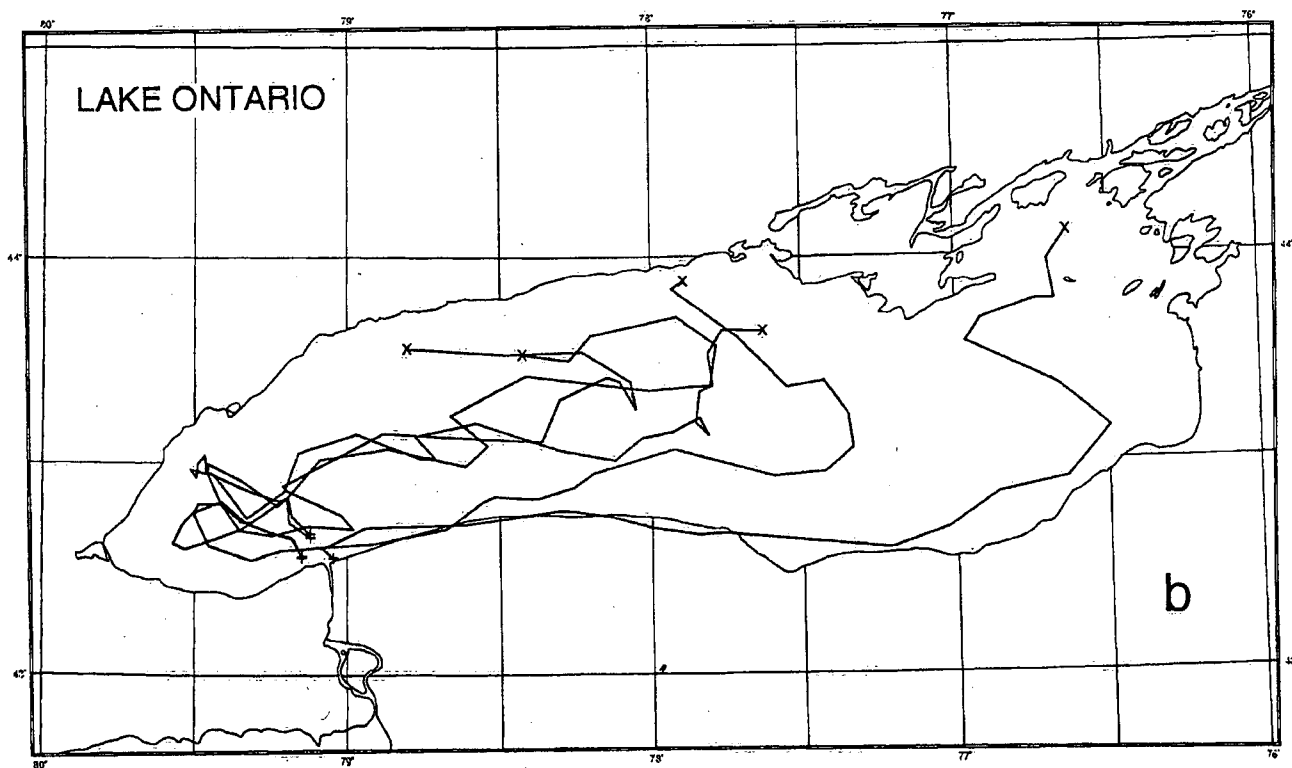
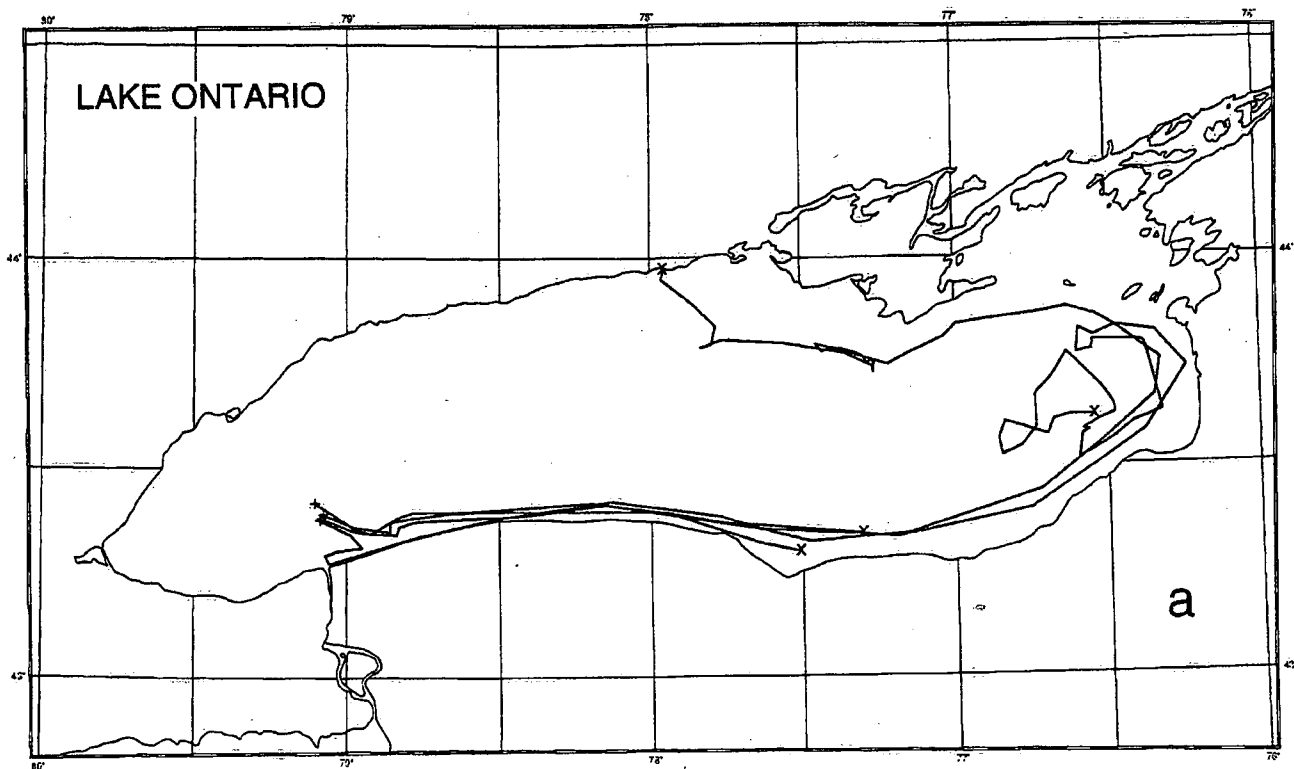


Fig. 6: Trajectories of surface drifters deployed on (a) June 5, 1985 and (b) September 18, 1985. The launch position is indicated by '+' and end position by 'x'

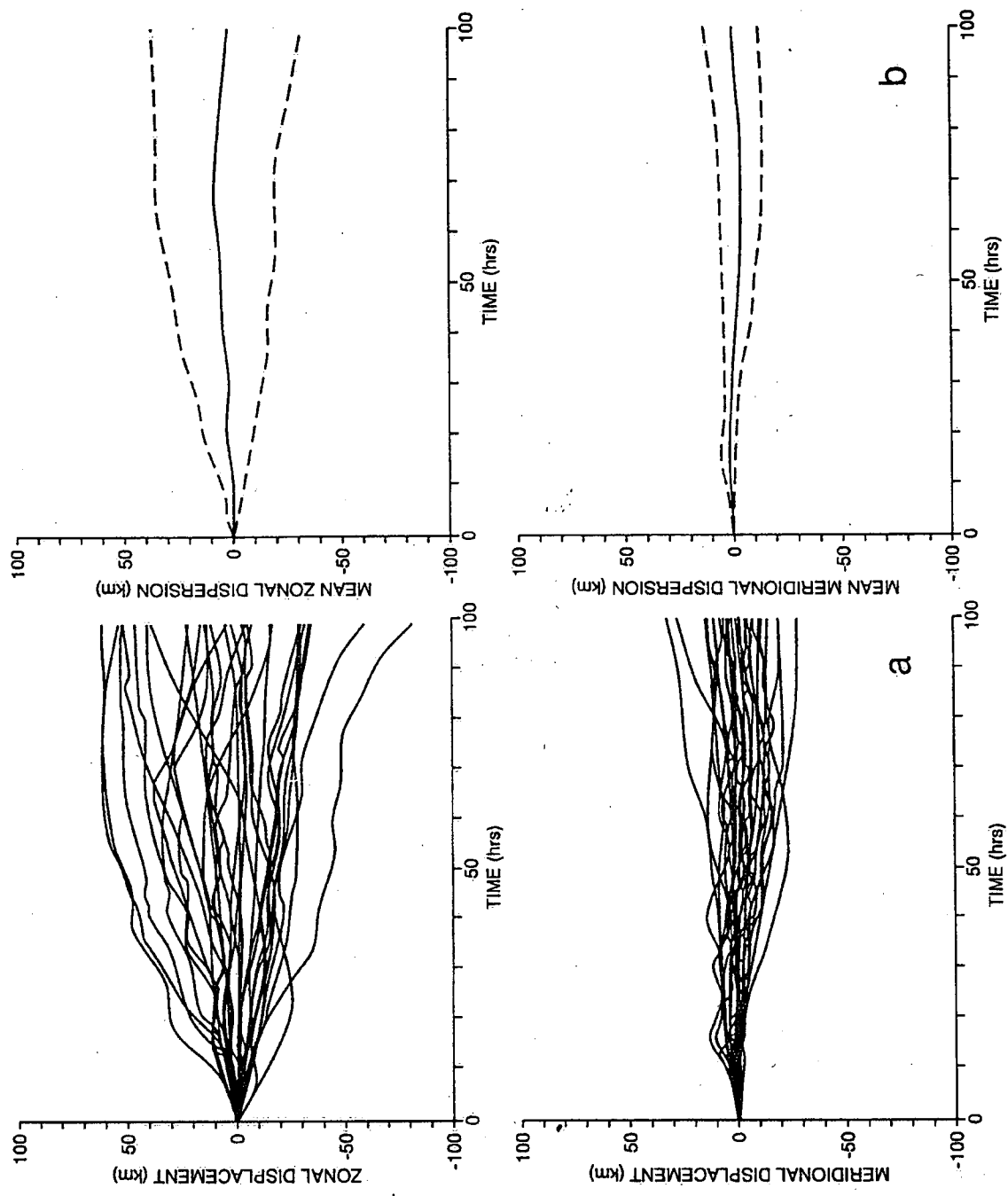


Fig. 7: (a) Zonal and meridional displacements versus time after deployment of 32 segmented drifter tracks from September 1985 experiment. (b) The mean displacements (solid line) and associated rms intervals (dotted envelopes) are also shown.

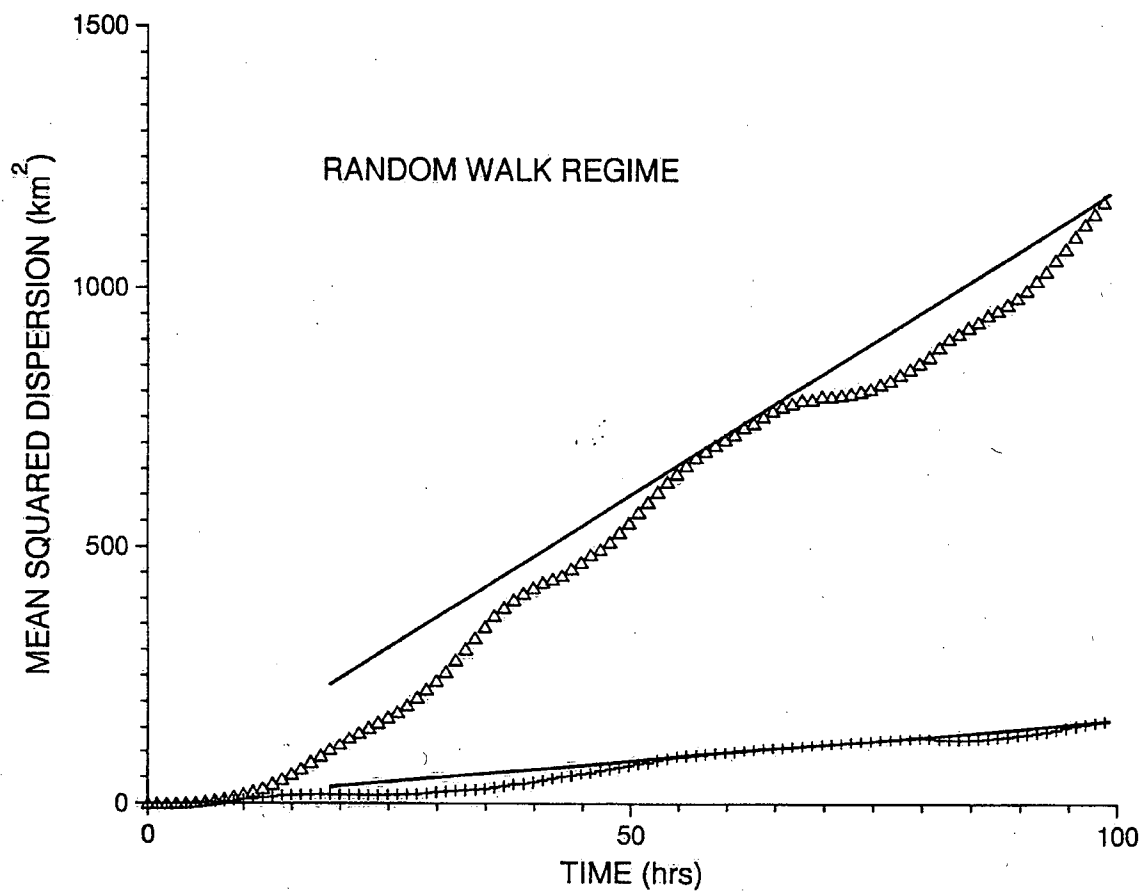


Fig. 8: Plot of mean-square dispersion versus time for the random walk regime. Symbols (triangle = zonal, cross = meridional) represent the observations. Taylor's theorem (eqn. 3.7) predicts the dispersion depicted by the solid line.

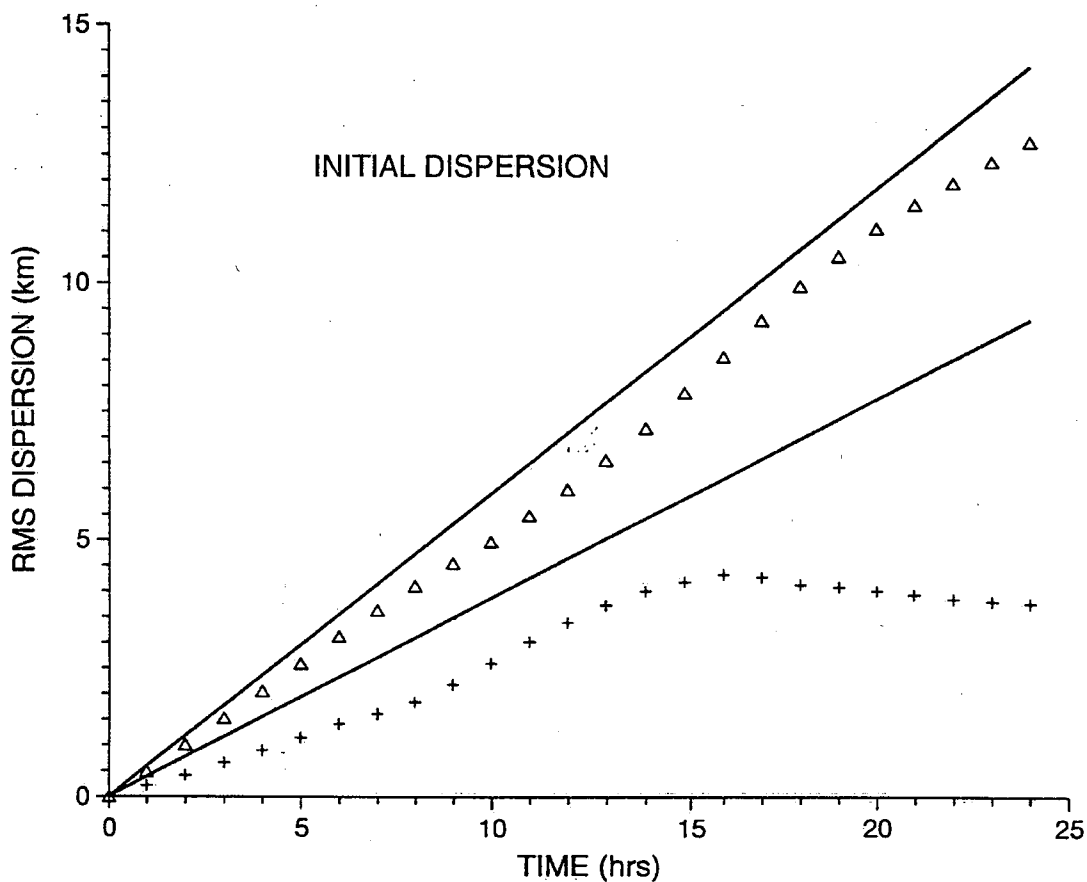


Fig. 9: Plot of root-mean-square dispersion versus time for the initial dispersion regime. Symbols (triangle = zonal, cross = meridional) represent the observations. Taylor's theorem (eqn. 6) predicts the dispersion depicted by the solid line.

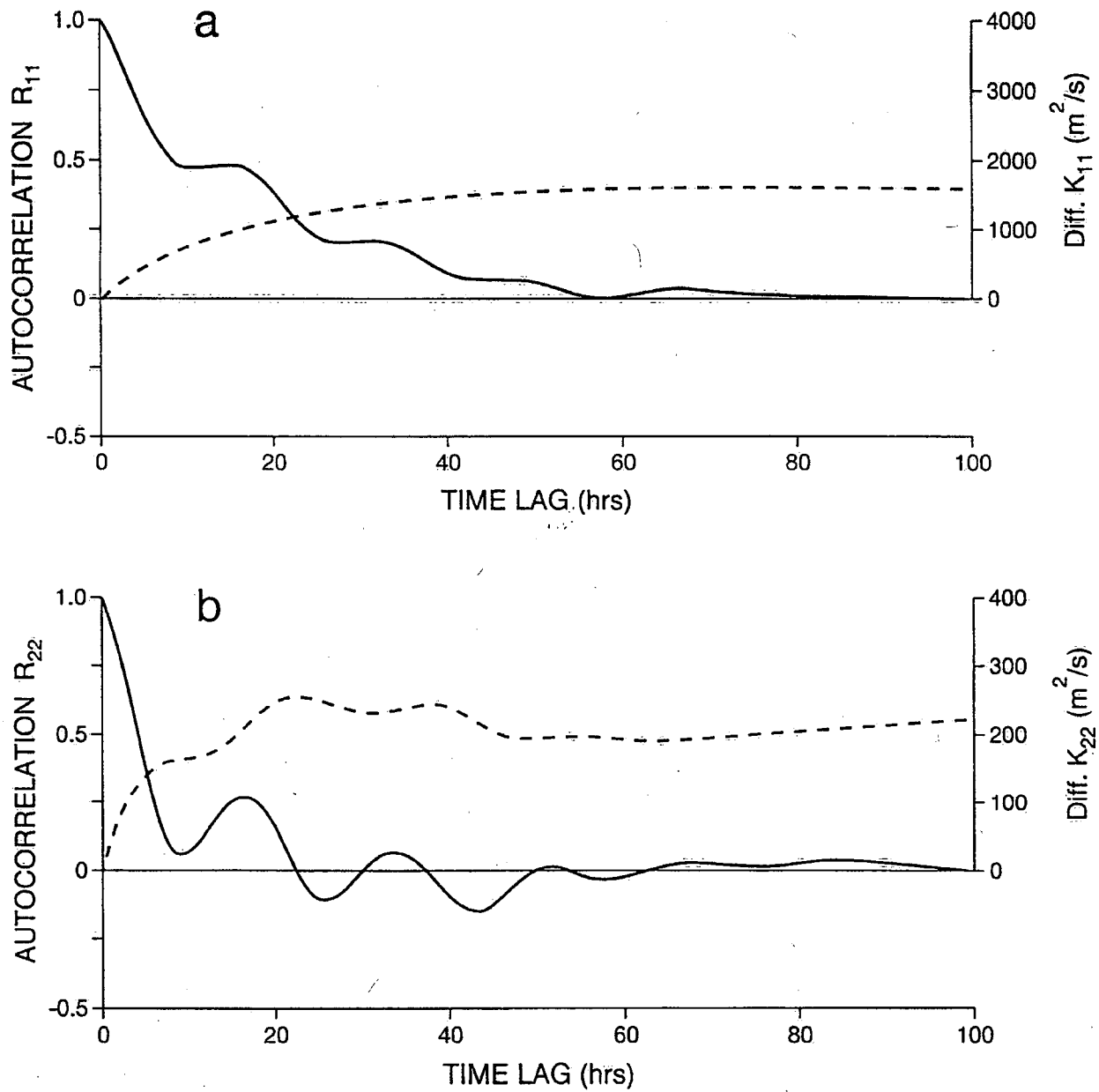


Fig. 10: Lagrangian autocorrelation functions and diffusivities as a function of time lag for the (a) zonal and (b) meridional directions. (Single-particle analysis.)

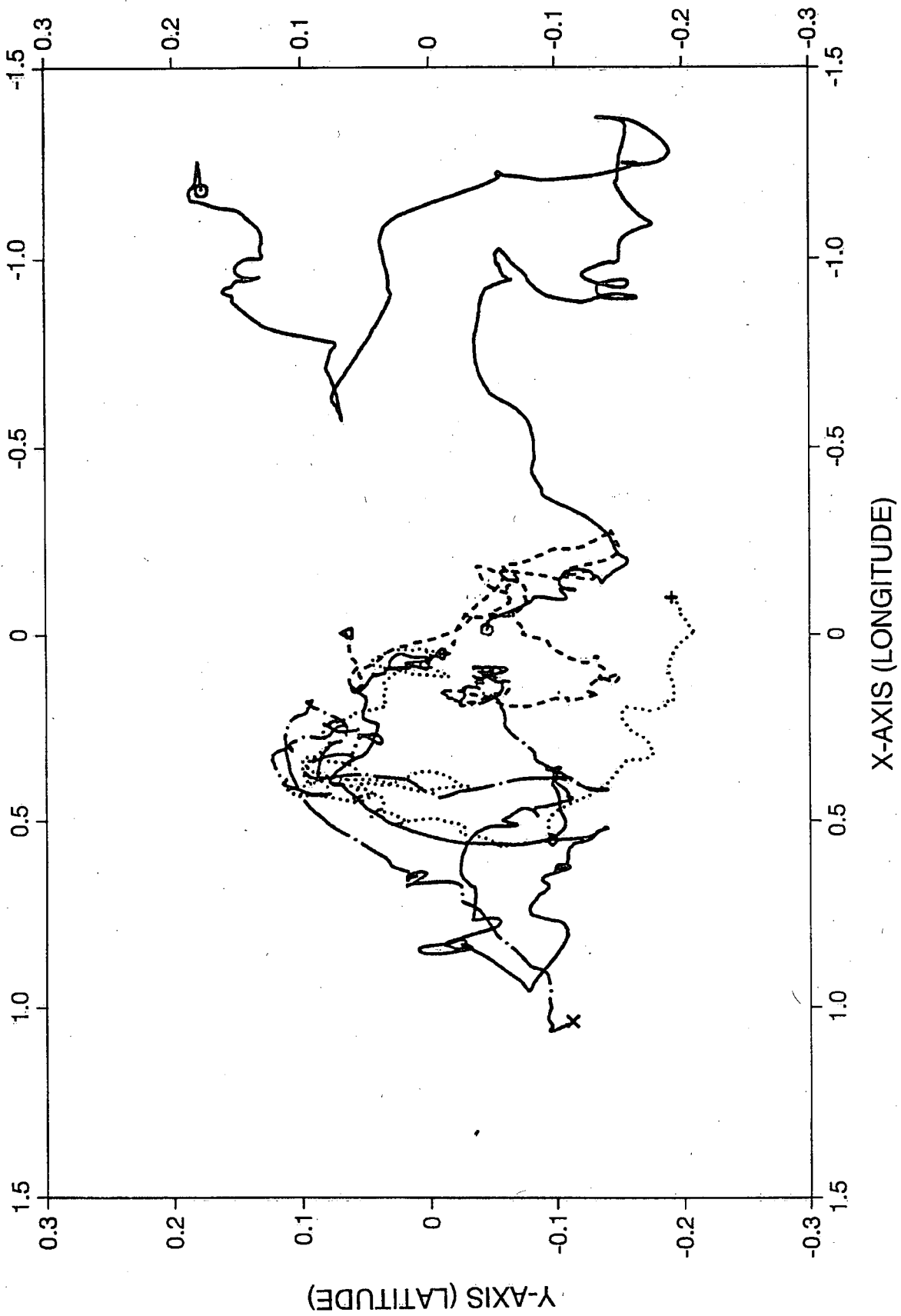


Fig. 11: Positions of drifters relative to the cluster centroid for September 1985 experiment.

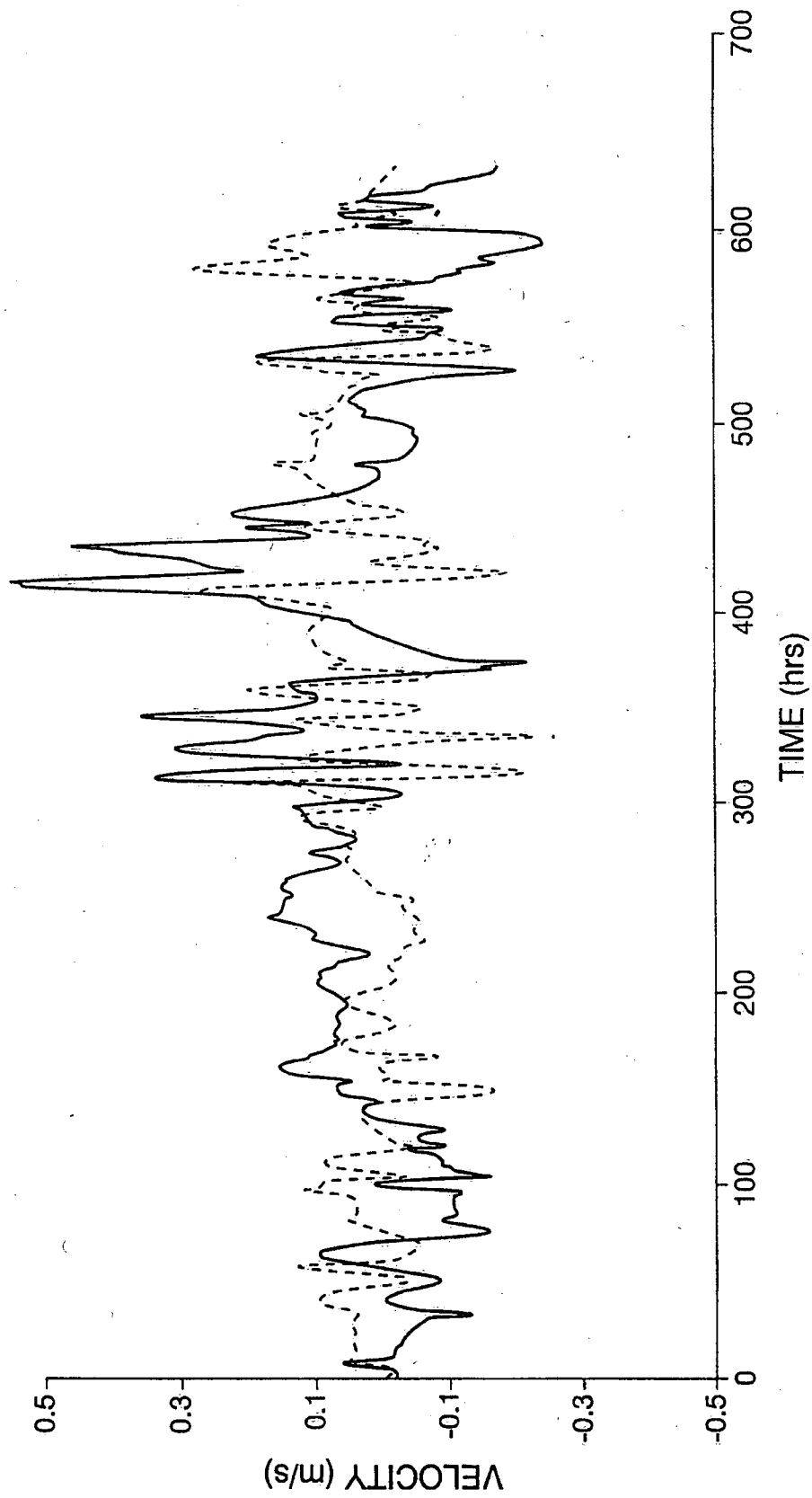


Fig. 12: Plot of velocity time series of the cluster centroid.

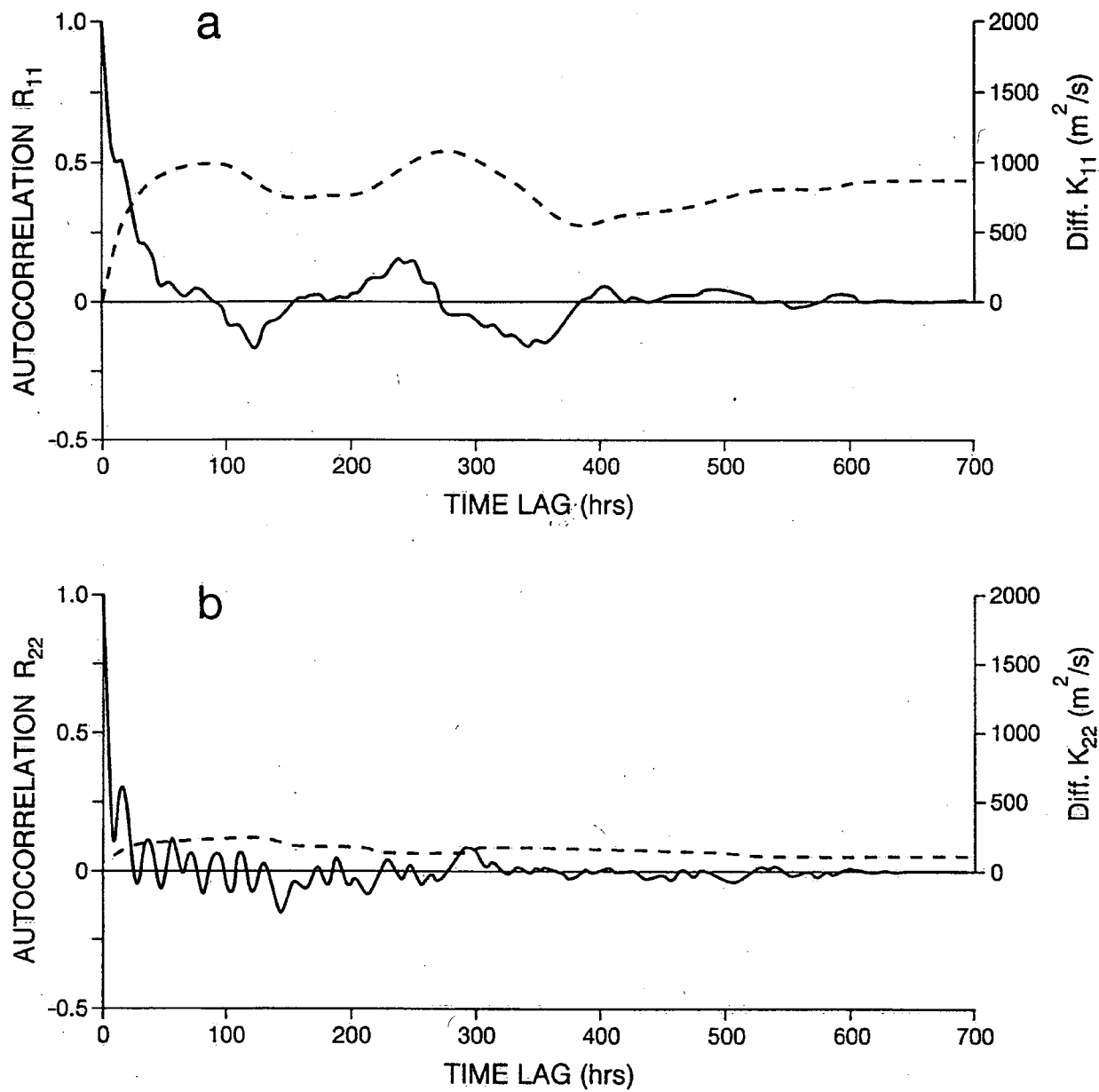


Fig. 13: Lagrangian autocorrelation functions and eddy diffusivities as a function of time lag for the (a) zonal and (b) meridional directions. (Cluster analysis.)

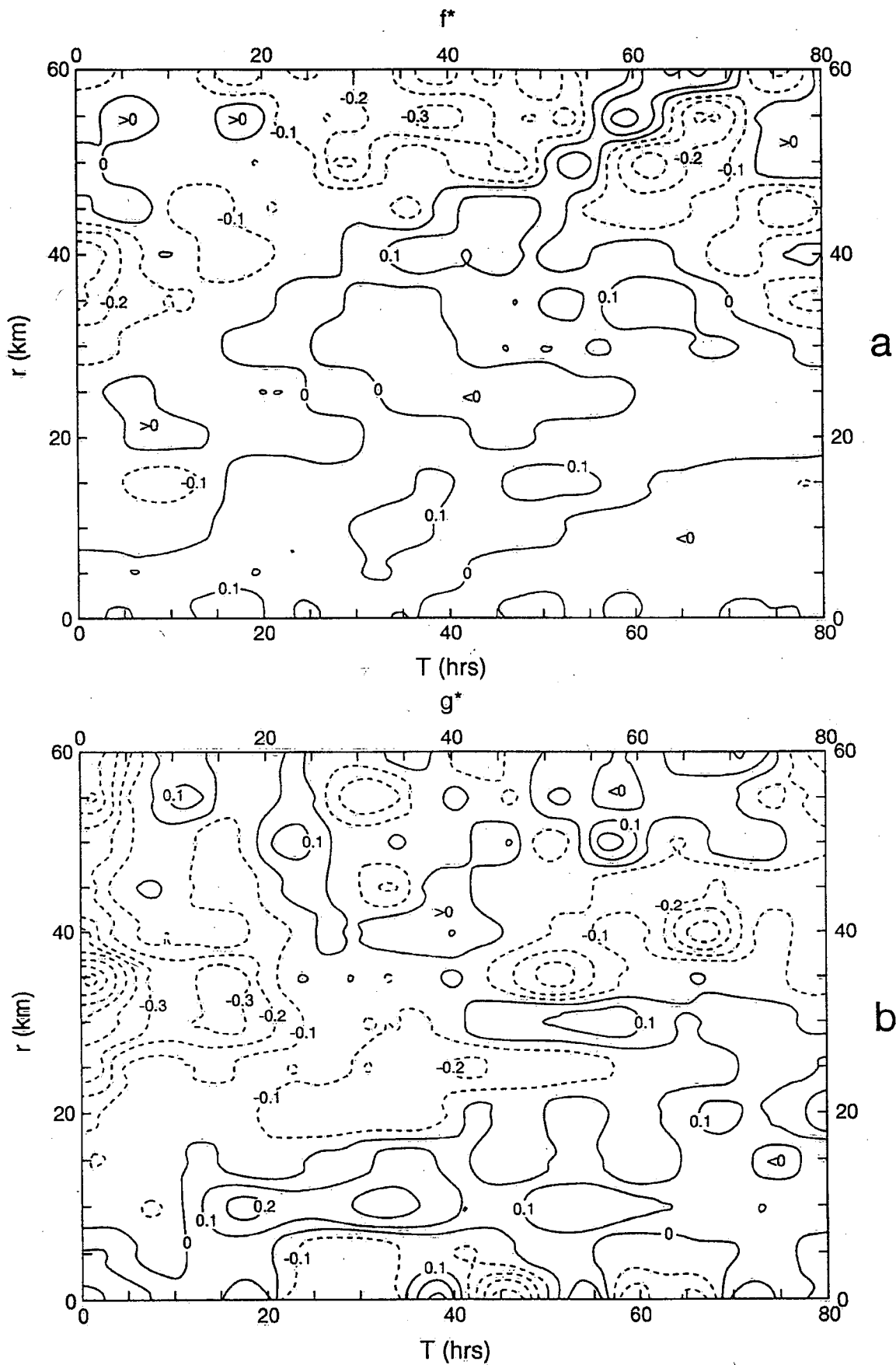


Fig. 14: Contour plots of Eulerian correlations f^* and g^* as functions of time and space lags, for September 1985 experiment. Areas of positive and negative correlations are designated by solid and dashed lines.

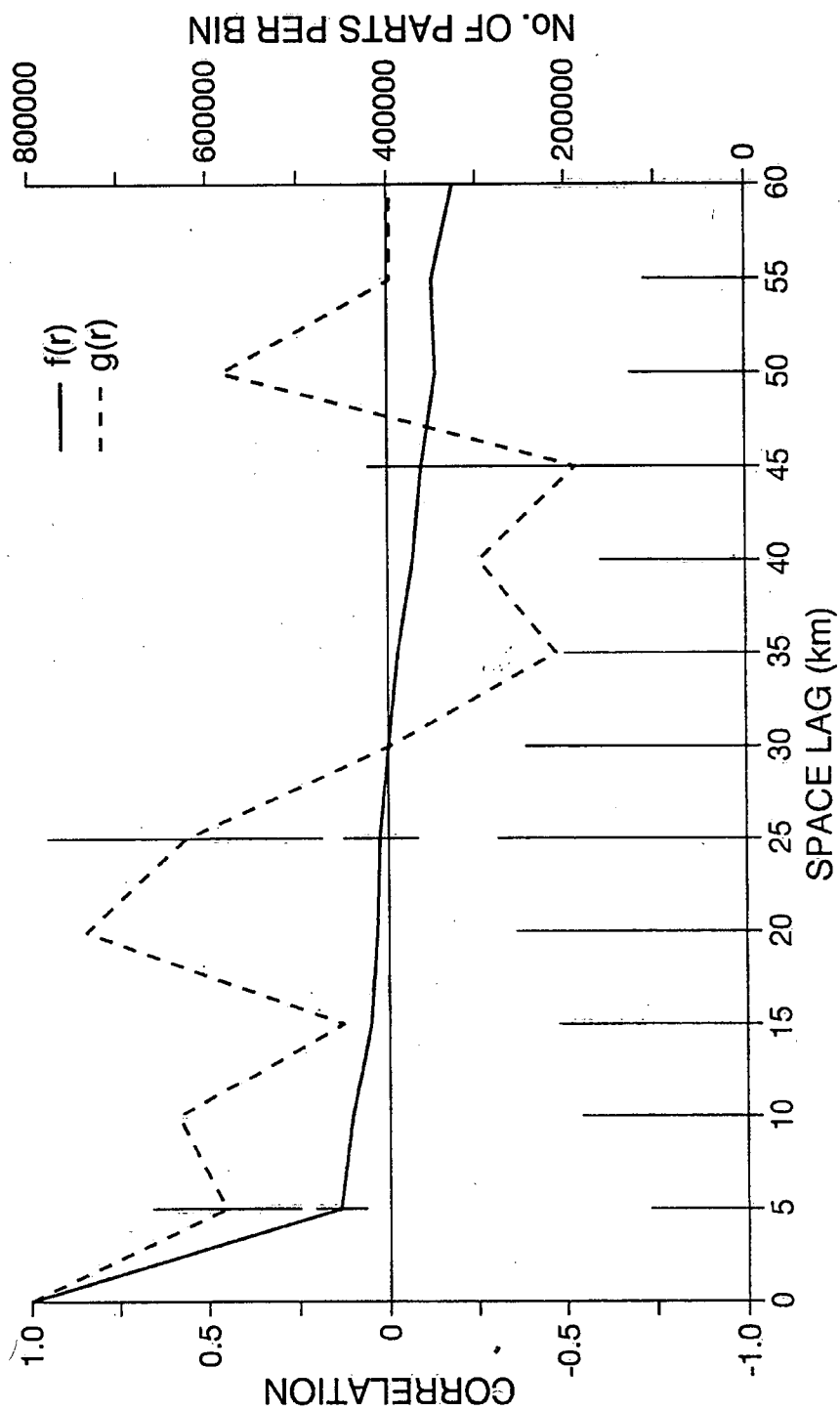


Fig. 15: Plots of Eulerian spatial correlations f and g as functions of space lag. Error bars represent $\pm \sigma$ about the mean value.

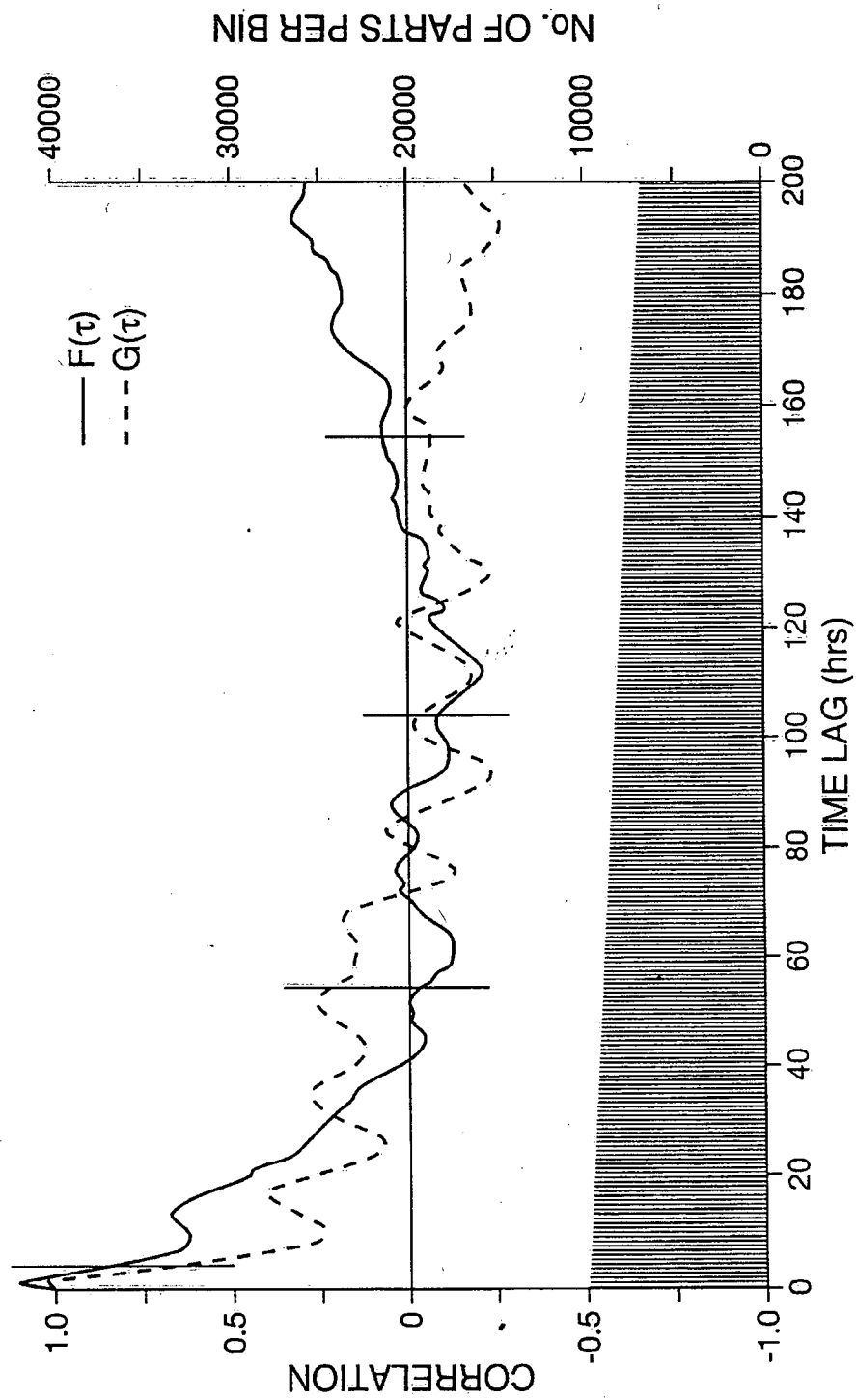


Fig. 16: Plots of Eulerian temporal correlations F and G as functions of time lag. Error bars represent $\pm \sigma$ about the mean value.

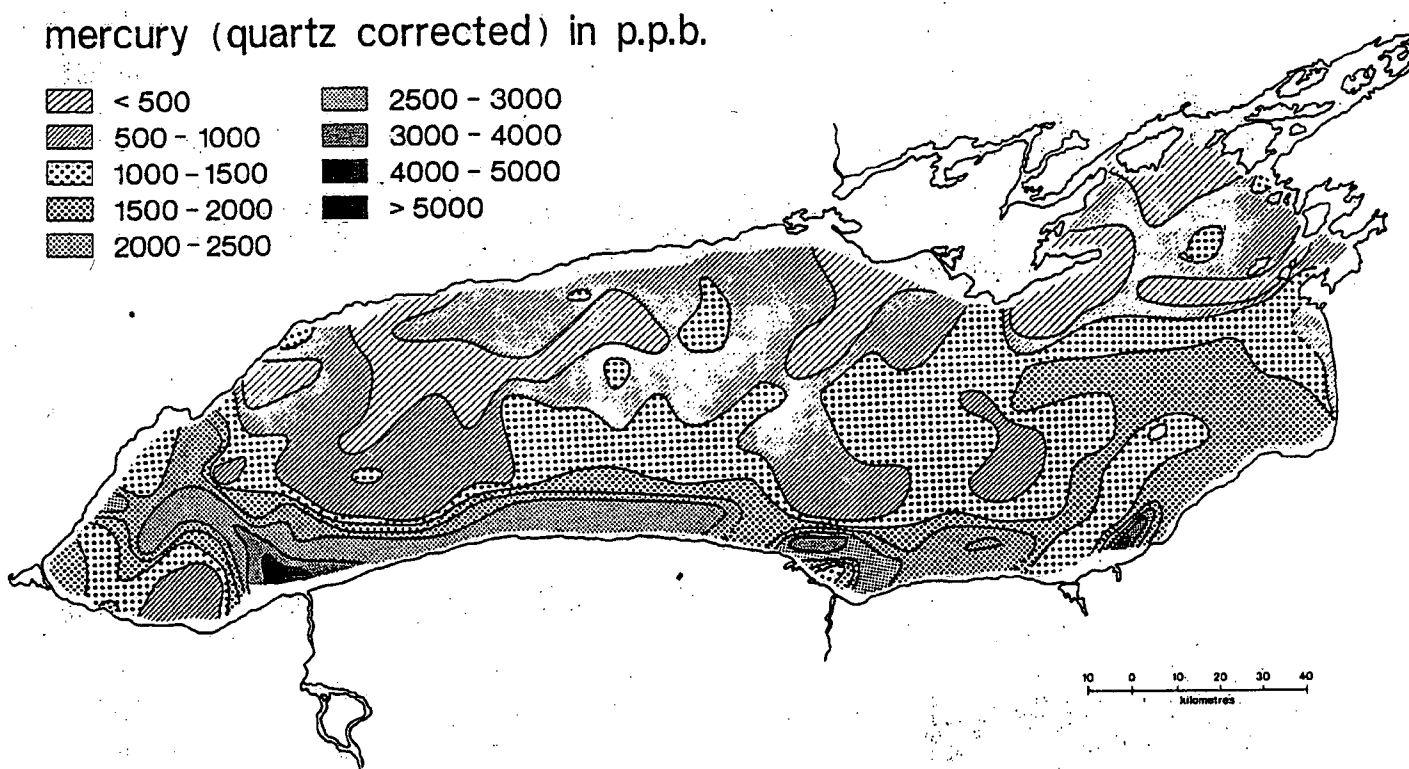
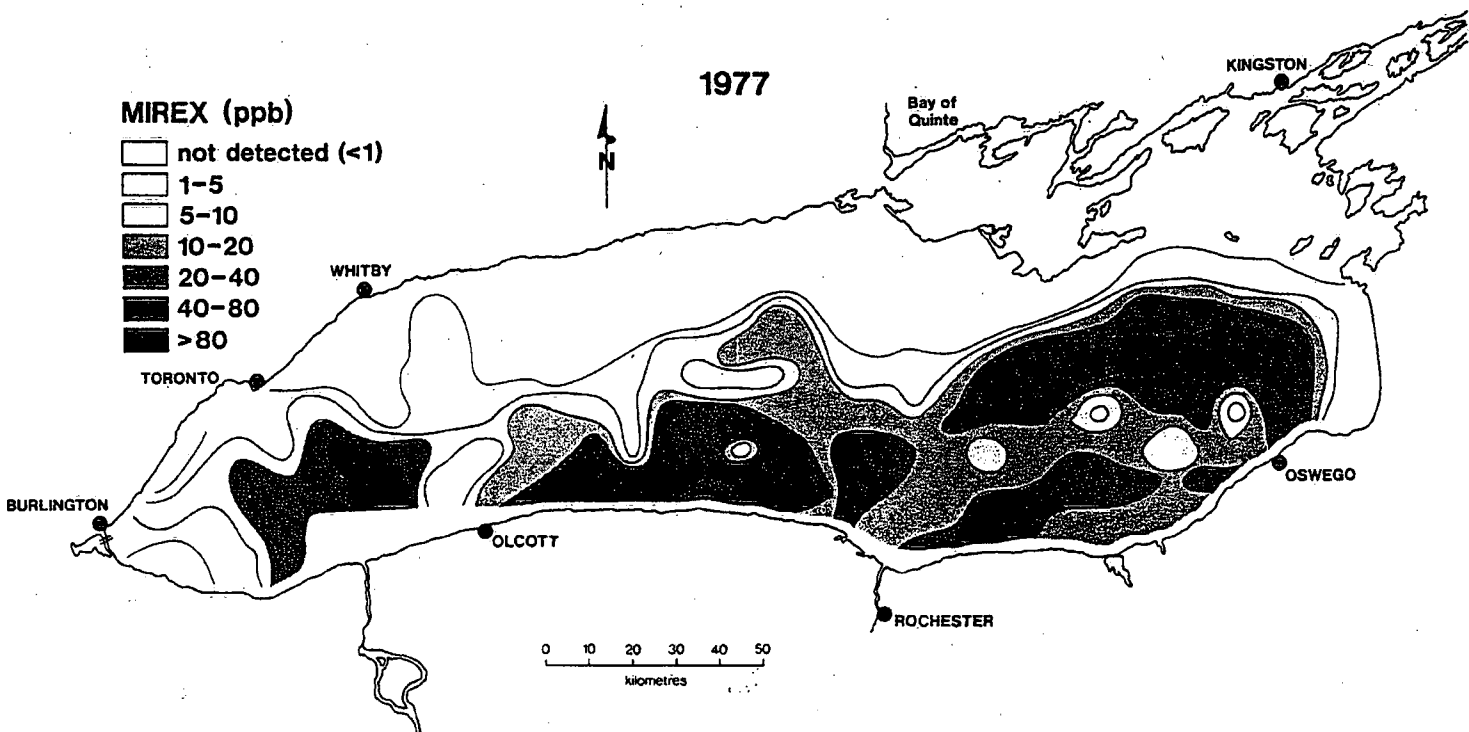


Fig. 17: Distribution of Mirex and mercury in Lake Ontario sediments (from Thomas 1983).

Environment Canada Library, Burlington



3 9055 1017 8254 7



Environment
Canada

Environnement
Canada

Canada

Canada Centre for Inland Waters

P.O. Box 5050
867 Lakeshore Road
Burlington, Ontario
L7R 4A6 Canada

National Hydrology Research Centre

11 Innovation Boulevard
Saskatoon, Saskatchewan
S7N 3H5 Canada

St. Lawrence Centre

105 McGill Street
Montreal, Quebec
H2Y 2E7 Canada

Place Vincent Massey

351 St. Joseph Boulevard
Gatineau, Quebec
K1A 0H3 Canada

Centre canadien des eaux intérieures

Case postale 5050
867, chemin Lakeshore
Burlington (Ontario)
L7R 4A6 Canada

Centre national de recherche en hydrologie

11, boul. Innovation
Saskatoon (Saskatchewan)
S7N 3H5 Canada

Centre Saint-Laurent

105, rue McGill
Montréal (Québec)
H2Y 2E7 Canada

Place Vincent-Massey

351 boul. St-Joseph
Gatineau (Québec)
K1A 0H3 Canada